Aust. J. Phys. Astrophys. Suppl., 1975, No. 37, 1–38

408 and 5000 MHz Observations of 28 New Galactic Supernova Remnants

D. H. Clark,[A] *J. L. Caswell*[B] *and Anne J. Green*[C]

[A] School of Physics, University of Sydney, Sydney, N.S.W. 2006.
[B] Division of Radiophysics, CSIRO, P.O. Box 76, Epping, N.S.W. 2121.
[C] Max-Planck-Institut für Radioastronomie, Auf dem Hügel 69, D53 Bonn 1, Germany.

Abstract

High-resolution contour maps of surface brightness at 408 and 5000 MHz are presented for 28 new galactic SNRs.

Introduction

The list of galactic radio sources believed to be the remnants of supernovae has increased dramatically in recent years, and the early catalogues of Milne (1970) and Downes (1971) have now been extensively supplemented by the identification of 27 new southern remnants reported by Clark *et al.* (1973). Furthermore, many of the uncertain identifications in the catalogues have been corrected by, amongst others, Shaver and Goss (1970), Caswell (1972), Dickel and Milne (1972) and Caswell and Clark (1975, pp. 57–73 of this Supplement).

The sources listed by Clark *et al.* (1973) were classified as supernova remnants (SNRs) on the basis of their nonthermal spectra, proximity to the galactic plane, significant angular extent, and (where resolution permitted) recognizable characteristic shell structure. In the present paper, further details of these sources are presented. These details consist principally of maps of surface brightness obtained with the Molonglo cross radiotelescope at 408 MHz and with the Parkes 64 m radiotelescope at 5000 MHz. Observations of an additional source G12.0–0.1 are also presented which suggest that it is a new SNR. Most of the new SNRs are of lower surface brightness than those of the Milne (1970) and Downes (1971) catalogues, so that considerable care was required in the definition of the extent of the sources and the estimation of their flux densities and spectra. However, the wide separation in frequency and the high resolution of the present observations allow the new SNR classifications to be made with a high degree of confidence.

The work described here forms part of a cooperative program undertaken between the University of Sydney and the Division of Radiophysics, CSIRO, to search for 'new' SNRs, to obtain high quality data for known SNRs, and to investigate some suggested SNR candidates for which the evidence is poor.

Observations

The 408 MHz Molonglo cross observations were taken from the high-resolution galactic survey completed by Green (1972). It was from this survey that an initial list of SNR suspects was prepared. The flux density scale used was that of Wyllie (1969), and during each observing session a number of standard sources from Hunstead's (1971, 1972) lists were measured for flux density and position calibration purposes.

The positional accuracy is believed to be everywhere better than 0′.5 arc. The 408 MHz contour maps of full-beam brightness temperature were produced by the KDF9 computer of the Basser Computing Centre, University of Sydney, using a program developed by D. F. Crawford. The original data, sampled every 3 s, were convolved with a filtering function to produce points every 6 s in a 1950.0 coordinate system. Since this final data grid was approximately at the Nyquist sampling points, band-limited interpolation was used to derive the contour lines. The zero level for the contours on each map was taken to be the level of lowest emission on that map, and was generally between 100 and 300 K above absolute zero (Green 1972). The zero level often did not coincide with the boundary of the SNR, and corrections for gradients in the background were sometimes necessary for the flux density estimates.

The 5000 MHz observations were made in April 1973 with the Parkes 64 m radio-telescope. The fields of interest were mapped by scanning in right ascension or declination, the choice being made on the basis of the ease of determining a suitable baselevel. Adjacent scans were spaced by half a beamwidth (2′ arc), and the primary calibrator for the system was Hydra A, for which a flux density of 13.5 Jy* was assumed. On each scan, filtering (which broadened the response by 10%) and removal of a linear sloping baseline were done by the on-line PDP-9 computer, with the final contour maps being prepared by hand from the computer-produced scans. On each 5000 MHz map the dashed 'zero' contour denotes the baselevel used to calculate the integrated flux density. The extent of the integration is also defined by this contour, except where the 408 MHz map shows that there are confusing unrelated sources adjacent to the SNR. In these latter cases the integration has been truncated in the directions of the confusing sources so as to agree with the 408 MHz angular extent. Positional errors of ~0′.5 arc may be present owing to telescope pointing uncertainties and the fact that no nearby positional calibration sources were observed.

At both 408 and 5000 MHz the intensity errors are believed to be generally less than 10%, and errors of relative intensity at the two frequencies are thus less than 20% for sources with well-defined boundaries. Even where confusing sources are present, we believe that close comparison of the maps has allowed us to achieve errors of <0.1 in spectral index ($<28\%$ error in the relative intensities). Some difficult cases are discussed in more detail in the following section.

Results

The parameters for the 27 sources suggested by Clark *et al.* (1973) as SNRs, together with G12.0–0.1, are summarized in Table 1. The contour maps are given in Figs 1–27 at the end of the paper (two SNRs being present on Fig. 16), with the 408 MHz map preceding the 5000 MHz map. The maps are all approximately equiangular and all maps are drawn to the same scale. The contour unit CU of brightness temperature (K) averaged over the beam solid angle is given in each 408 MHz map and in the caption to each 5000 MHz map. Contours enclosing local intensity minima have inward-pointing tick marks.

At 408 MHz the half-power beamwidths HPBW are 2′.86 and 2′.86 $\sec(\delta+35^\circ.5)$ arc in right ascension and declination respectively, and the beam shape is shown as a shaded ellipse. A point source of flux density 1 Jy at 408 MHz gives a peak beam brightness temperature of 257 $\sec(\delta+35^\circ.5)$ K.

* 1 jansky (Jy) = 10^{-26} W m^{-2} Hz^{-1}.

Table 1. Flux densities and spectral indices for 28 'new' SNRs

Source number	S_{408} (Jy)	S_{5000} (Jy)	Spectral index α_{408}^{5000}
G293.8+0.6	9.0	2.1	−0.58
G296.1−0.7	6.9	>0.74	−0.72
G299.0+0.2	12.6	4.7	−0.39
G302.3+0.7	7.5	3.0	−0.36
G308.7+0.0	16.7	7.0	−0.35
G309.2−0.6	10.0	3.9	−0.37
G309.8+0.0	26.4	7.4	−0.51
G315.4−0.3	15.9	4.9	−0.47
G321.9−0.3	18.3	7.8	−0.34
G323.5+0.1	4.2	1.5	−0.41
G327.1−1.1	10.6	4.3	−0.36
G330.2+1.0	8.6	4.0	−0.30
G335.2+0.1	27.1	8.6	−0.46
G337.2−0.7	3.8	0.70	−0.67
G339.2−0.4	7.5	4.5	−0.20
G340.4+0.4	8.2	2.9	−0.41
G340.6+0.3	7.0	2.8	−0.36
G344.7−0.1	4.7	1.3	−0.51
G346.6−0.2	14.9	4.3	−0.49
G350.1−0.3	10.7	1.7	−0.73
G350.0−1.8	49.5	13.6	−0.51
G351.2+0.1	8.1	3.1	−0.38
G352.7−0.1	9.6	2.3	−0.57
G355.9−2.5	12.3	3.4	−0.51
G11.4−0.1	9.4	2.8	−0.48
G12.0−0.1	6.6	1.1	−0.71
G15.9+0.2	7.7	1.9	−0.56
G24.7−0.6	12.3	3.6	−0.49

At 5000 MHz the effective half-power beamwidth (after filtering) is 4′.4 arc in the direction of scanning (the direction of the 5000 MHz scan is given in the caption to the map) by 4′.0 arc at right angles to this direction. A point source of 1 Jy at 5000 MHz gives a peak beam brightness temperature of 0.75 K.

We have searched for possible associations of these SNRs with X-ray sources from the third Uhuru catalogue (Giacconi *et al.* 1974) but none appear to be significant. However, a small-diameter radio source at the edge of Fig. 9 appears to be a probable identification with 3U1516−56 (see G321.9−0.3 below). Each SNR is considered individually below, where a revision is made of some of the source parameters given in the preliminary paper by Clark *et al.* (1973). In three cases the source names have been modified to correspond better with the centre of the area covered by the source.

G293.8+0.6 (Fig. 1)

The amorphous source G293.8+0.6 displays at 408 MHz a central peak embedded in a region of low surface brightness and ill-defined extent; the absence of prominent peripheral brightening is unusual for an SNR. Both peak brightness and integrated flux density indicate that this source is nonthermal with $\alpha = -0.58$, where $S \propto \nu^{\alpha}$. For comparison we note that more than 80% of previously known galactic SNRs have α in the range −0.3 to −0.6.

G296.1−0.7 (*Fig. 2*)

This source was designated G296.0−0.6 by Clark *et al.* (1973). The present 408 MHz map shows a quite well-defined shell of emission which is brightest in the south-west quadrant (i.e. to the south and at smaller right ascension). The zero level for the 5000 MHz map, defined by the dashed curve, does not enclose the north-east prominence evident on the 408 MHz map. The exclusion of this feature in the estimate of the 5000 MHz flux is partly responsible for the steep spectral index (−0.89) which we originally obtained for this source. An improved estimate of the spectral index is −0.72, obtained from the ratio of peak surface brightnesses measured in the south-west.

G299.0+0.2 (*Fig. 3*)

The 408 MHz map of G299.0+0.2 shows what is apparently a part-shell source with southern and north-eastern peaks. However, the southern peak, which dominates the 5000 MHz map, is apparently thermal and makes the maximum contribution to the 5000 MHz flux. The north-eastern peak and the arc stretching to it are both nonthermal but appear to have different spectral indices. The mean spectral index of −0.39 refers to all three features, since they are not readily separated.

G302.3+0.7 (*Fig. 4*)

At 408 MHz, G302.3+0.7 shows up as a well-defined shell of low surface brightness dominated by north-east and south-west arcs. At 5000 MHz the more prominent features are still evident. The integrated flux densities give a spectral index of −0.36.

G308.7+0.0 (*Fig. 5*)

G308.7+0.0 is an amorphous source with north-eastern elongation. The integrated flux densities give a spectral index of −0.35. The position of a type 1 OH emitter is shown by a cross on the 408 MHz map. Probably some emission in this region is thermal, but the overall spectrum is sufficiently steep to be reliably nonthermal.

G309.2−0.6 (*Fig. 6*)

The 408 MHz map of G309.2−0.6 shows what could be either portions of an incomplete shell source or, alternatively, two separate nonthermal sources (similar to the proposed SNRs CTB 37A and 37B). The 5000 MHz map is confused to the north with a thermal region, which probably corresponds to the optical nebula RCW 80. However, the northern boundary was defined by reference to the 408 MHz map, with the flux density estimate thus obtained giving a mean spectral index for the complete 408 MHz object of −0.37. Individually the two portions have spectra similar to this mean value, as may be inferred from their similar relative intensities at 408 and 5000 MHz.

G309.8+0.0 (*Fig. 7*)

The point source at R.A. $13^h47^m06^s$, Dec. $-61°46'$ makes the 408 MHz map of G309.8+0.0 look rather complex. The 5000 MHz map more clearly depicts a part-shell source with southern prominences. The absence of the point source on the 5000 MHz map indicates that its spectral index is steeper than −1.0 and strikingly different from the value of −0.51 obtained for the complete remnant. The steep spectrum of the point source suggested that it might be a pulsar (approximately at the centre of the SNR), but observations at 630 MHz have failed to detect any pulses

(M. M. Komesaroff, personal communication); thus the source is either a pulsar with period shorter than that searched for ($<0^s.1$) or quite probably a background extragalactic source.

G315.4–0.3 (*Fig. 8*)

The point source at R.A. $14^h33^m12^s$, Dec. $-60°16'$ was originally included in the 408 MHz flux density of G315.4–0.3. The fact that it is not prominent on the 5000 MHz map suggests that it may be extragalactic. Extraction of the 1.2 Jy point source from the 408 MHz flux density produces a spectral index of –0.47 for the remainder. The feature at R.A. $14^h31^m18^s$, Dec. $-60°26'$ has a much flatter spectrum than the source as a whole, and may be thermal.

G321.9–0.3 (*Fig. 9*)

The SNR G321.9–0.3 shows up at both frequencies as a well-defined shell source with maximum emission from the western edge. The spectral index is –0.34. The feature at R.A. $15^h16^m34^s$, Dec. $-57°32'$ on the 408 MHz map is possibly a sidelobe of a neighbouring point source at R.A. $15^h16^m32^s$, Dec. $-57°56'55''$.

The best estimate of the position of the X-ray source 3U1516–56 (≡ Cir X-1) has recently been revised to R.A. $15^h16^m47^s$, Dec. $-56°59'28''$ (Jones *et al.* 1974) and its error box of approximately $2' \times 1'$ arc overlaps a small-diameter source seen at the north edge of the 408 MHz map. The radio source was also detected at 5000 MHz and, although contours around this source have not been drawn, the original observations extended to the north of the map and allowed a flux density and position to be measured. The measurements at 408 MHz yielded a position at R.A. $15^h16^m47^s.3$, Dec. $-56°59'44''$, with S_{408} = 0.46 Jy; the 5000 MHz position was R.A. $15^h16^m46^s.4$, Dec. $-56°59'54''$, with S_{5000} = 0.25 Jy. Thus we obtain $\alpha_{408}^{5000} = -0.25$. The X-ray source shows large intensity changes in seconds. On the two occasions when the radio source was observed at 408 MHz (March and September 1970) it showed the same flux density. The identification must remain tentative pending improved position measurements; apart from the proximity of the small-diameter radio and X-ray sources to the SNR, there are at present no strong additional grounds for associating them with the SNR.

G323.5+0.1 (*Fig. 10*)

What appears as a small shell source (G323.5+0.1) at 408 MHz is lost in the confusion of neighbouring thermal regions to the south and west at 5000 MHz. However, superposition of the 408 and 5000 MHz maps allowed a determination of the flux density believed to be attributable to the SNR at 5000 MHz, giving S_{5000} = 1.5 Jy; this is a more precise estimate than the limits given by Clark *et al.* (1973), and the resulting spectral index is –0.41.

G327.1–1.1 (*Fig. 11*)

This source was designated G327.2–1.0 by Clark *et al.* (1973). The present maps at the two frequencies were difficult to reconcile for this source. The 408 MHz map depicts a shell source with a strong peak in emission in the north-eastern quadrant. The 5000 MHz map, while also exhibiting this peak, shows a westerly extension towards what is a low-intensity region at 408 MHz, with no evidence of the shell structure. The integrated flux densities give a mean spectral index for the complete source of –0.36.

However, this value should be interpreted with caution, since the complex variation of spectral index across the source indicated by the dissimilarity of the maps may result from the superposition of unrelated sources.

G330.2+1.0 (*Fig. 12*)

The 5000 MHz map of G330.2+1.0 also shows some confusion, in this case with a thermal region on its eastern border. Careful definition of the extent of flux density integration at the two frequencies gave a spectral index of −0.30.

G335.2+0.1 (*Fig. 13*)

The well-defined shell source G335.2+0.1 has a spectral index, obtained from the integrated flux densities, of −0.46. The similarity of the two maps indicates that the spectral index is nearly constant over the complete remnant. A pronounced north-west to south-east gradient in the background radiation is evident in the 408 MHz map but was corrected for in the estimate of the 408 MHz flux density.

G337.2−0.7 (*Fig. 14*)

Our resolution was insufficient to determine any structure in G337.2−0.7. However, its nonthermal nature ($\alpha = -0.67$), uniform broadening and proximity to the galactic plane establish this source as a probable SNR.

G339.2−0.4 (*Fig. 15*)

Because of its relatively flat spectrum, G339.2−0.4 must remain the most doubtful of the present SNR classifications, although a number of accepted SNRs, such as G5.3−1.0 ≡ A4 (Milne and Dickel 1971), have equally flat spectra. By carefully defining the limits of integration on the two maps, we obtained a spectral index of −0.20 for the source with centroid R.A. $16^h41^m50^s$, Dec. $-46°03'$. Our assessment of the possible errors suggests that this estimate is probably not consistent with a thermal spectral index of −0.1. At the position of G339.2−0.4 an approximately semi-circular arc (diameter ~6′ arc) of diffuse optical emission can be seen on a red print taken by T. A. Matthews with the Palomar 48-inch Schmidt (in a series of photographs commonly referred to as the 'Matthews extension of the Palomar Sky Survey'). The identification with the radio source seems certain on account of both positional agreement and angular extent. Thus investigation of the optical feature may prove conclusively whether the object is indeed an SNR rather than an HII region. This general area of sky is of particular interest; it contains the recently discovered Parkes pulsar 1641−45, indicated by a cross on the 408 MHz map where it shows up as a 0.5 Jy point source, and the X-ray source 3U1642−45 (≡ 2U1641−45) which lies 20′ arc north of the map boundary but is probably unrelated to the SNR.

G340.6+0.3 and G340.4+0.4 (*Fig. 16*)

The two most prominent sources seen on the 408 MHz map are separate supernova remnants. The SNR G340.4+0.4 has $\alpha = -0.41$ and the SNR G340.6+0.3 has $\alpha = -0.36$. The third source G340.2+0.5 seen on the maps is thermal.

G344.7−0.1 (*Fig. 17*)

The 408 MHz observations of G344.7−0.1 show some suggestion of a peripheral brightness distribution indicative of a shell structure. The source has $\alpha = -0.51$.

G346.6–0.2 (*Fig. 18*)

In the source G346.6–0.2 a clear shell structure is visible with the higher resolution of the 408 MHz map. The spectral index is –0.49.

G350.1–0.3 (*Fig. 19*)

This source was designated G350.0–0.3 by Clark *et al.* (1973). The present resolution was insufficient to detect any structure in this source. The distinct elongation at position angle 105°, with some indication of broadening perpendicular to this, together with the proximity to the galactic plane have led us to classify this source as an SNR rather than an extragalactic object, despite the quite steep spectrum (α = –0.73).

G350.0–1.8 (*Fig. 20*)

The source G350.0–1.8 may be only part of an old large SNR, the bright north-western ridge possibly resulting from interaction with a higher-density interstellar medium towards the galactic plane. Both the integrated flux density and peak brightness along the ridge indicate that this source is nonthermal, with spectral index –0.51. There are, however, different spectral features across the remnant, e.g. the bright region behind the ridge on the 5000 MHz map overlaps a region of low emission at 408 MHz.

G351.2+0.1 (*Fig. 21*)

The 408 MHz map of G351.2+0.1 shows an arc structure suggestive of a part-shell source. The spectral index was estimated to be –0.38.

G352.7–0.1 (*Fig. 22*)

The 5000 MHz map of G352.7–0.1 shows a neighbouring thermal source to the east, which is also evident on the 408 MHz map. The resolution of both maps was insufficient to show any definite structure in the suggested SNR source, which is non-thermal with estimated spectral index of –0.57.

G355.9–2.5 (*Fig. 23*)

The source G355.9–2.5 shows a well-defined part-shell structure at both frequencies, and has a spectral index of –0.51 which is constant over the remnant. From the 408 MHz surface brightness, an estimate of the distance to this SNR using the surface-brightness-linear-diameter relation of Clark *et al.* (1973) yields a value of 9.8 kpc. Its distance from the galactic plane is then calculated to be 430 pc (compared with the scale height for all SNRs of 110 pc (Mills 1974)). Thus apparently it is at a considerably greater distance from the plane than the other SNRs mapped here. It is similar in this regard to Kepler's SNR and since, in addition, both sources are probably quite near the galactic centre (in distance as well as direction), they may both lie in the nuclear bulge of the Galaxy.

G11.4–0.1 (*Fig. 24*)

The part-shell source G11.4–0.1 was reported in our previous paper (Clark *et al.* 1973) as having the relatively flat spectral index of –0.25. The 408 MHz map is badly contaminated by sidelobes from a strong neighbouring source at R.A. $18^h08^m35^s$, Dec. $-19°26'$, and the difficulty in estimating a background level results in a greater than usual uncertainty in the 408 MHz flux density. Reconstruction of the baselevel

in the vicinity of the source leads to a revised flux density of S_{408} = 9.4 Jy, which combined with the 5000 MHz flux density yields a spectral index of −0.48.

G12.0−0.1 (*Fig. 25*)

The source G12.0−0.1 was not included in our preliminary list of 'new' SNRs. The 408 MHz map shows two overlapping sources with peaks separated ~5′ arc. At 5000 MHz only the western peak (at R.A. $18^h09^m00^s$, Dec. $-18°37'30''$) is prominent. We conclude that this western peak is thermal with an angular diameter (deconvolved gaussian half-width) of 2′.4 arc and integrated flux densities of 2.9 and 2.2 Jy at 408 and 5000 MHz respectively. At 408 MHz the eastern peak (at R.A. $18^h09^m16^s$, Dec. $-18°38'20''$) has a flux density of 6.6 Jy and an angular diameter of 4′.5 arc. Although not easily measured at 5000 MHz, this feature appears to have a peak flux density of ~0.5 Jy corresponding to an integrated flux density (adopting the size measurement at 408 MHz) of 1.1 Jy. The spectral index is thus −0.71. In view of its nonthermal spectrum, significant angular size and low galactic latitude we conclude that this latter source is an SNR.

G15.9+0.2 (*Fig. 26*)

The resolution is sufficient only to show that the intensity gradient to the east of G15.9+0.2 is considerably greater than to the west. The spectral index of this nonthermal source is −0.56.

G24.7−0.6 (*Fig. 27*)

G24.7−0.6 appears as a part-shell source at both frequencies. The integrated flux densities give a spectral index of −0.49.

Conclusions

The sources mapped in this paper represent a significant increase in the number of galactic SNRs observed at southern declinations and, in particular, of older low surface-brightness remnants for which previous lists were incomplete. Using a revised surface-brightness-linear-diameter relation for estimating the distance to SNRs, Clark *et al.* (1973) showed that SNRs are more or less uniformly distributed over the galactic plane out to at least 10 kpc from the galactic centre. Many of the new SNRs mapped here lie in those regions of the Galaxy which are distant and generally beyond the sensitivity limits of earlier catalogues.

Although identification of SNRs solely on the basis of spectra and structure can lead to some uncertainties, other identification techniques, such as polarization observations and searching for H109α recombination line emission, would be inconclusive for radio sources of such low intensity as most of those discussed in this paper. By careful definition of the extent of emission and estimation of flux densities, most of the present identifications can be made with considerable confidence. However, the three sources G299.0+0.2, G339.2−0.4 and G350.1−0.3, although fulfilling the basic requirements of apparent nonthermal spectra and significant angular extent, remain more doubtful than the rest. Thus G299.0+0.2 comprises several possibly unrelated features, G339.2−0.4 has a spectrum that is quite flat, while the angular structure and steep spectrum of G350.1−0.3 indicate that it might be extragalactic.

Acknowledgments

The on-line computer program used in the 5000 MHz observations was written by Dr J. V. Wall and we thank him for modifying it to be especially suitable for our requirements. The Molonglo radio observatory is supported by grants from the Australian Research Grants Committee, the Sydney University Research Grants Committee, and the Science Foundation for Physics within the University of Sydney.

References

Caswell, J. L. (1972). *Aust. J. Phys.* **25**, 443.
Caswell, J. L., and Clark, D. H. (1975). *Aust. J. Phys. Astrophys. Suppl.* No. 37, 57.
Clark, D. H., Caswell, J. L., and Green, Anne J. (1973). *Nature* (*London*) **246**, 28.
Dickel, J. R., and Milne, D. K. (1972). *Aust. J. Phys.* **25**, 539.
Downes, D. (1971). *Astron. J.* **76**, 305.
Giacconi, R., *et al.* (1974). *Astrophys. J. Suppl. Ser.* **27**, 37.
Green, Anne J. (1972). Ph.D. Thesis, University of Sydney.
Hunstead, R. W. (1971). *Mon. Notic. Roy. Astron. Soc.* **152**, 277.
Hunstead, R. W. (1972). *Mon. Notic. Roy. Astron. Soc.* **157**, 367.
Jones, C., Giacconi, R., Forman, W., and Tananbaum, H. (1974). *Astrophys. J.* **191**, L71.
Mills, B. Y. (1974). Observational aspects of supernova remnants, Proc. IAU Symp. No. 60 (Reidel: Dordrecht, Holland).
Milne, D. K. (1970). *Aust. J. Phys.* **23**, 425.
Milne, D. K., and Dickel, J. R. (1971). *Nature Phys. Sci.* **231**, 33.
Shaver, P. A., and Goss, W. M. (1970). *Aust. J. Phys. Astrophys. Suppl.* No. 14, 133.
Wyllie, D. V. (1969). *Mon. Notic. Roy. Astron. Soc.* **142**, 229.

Manuscript received 5 September 1974

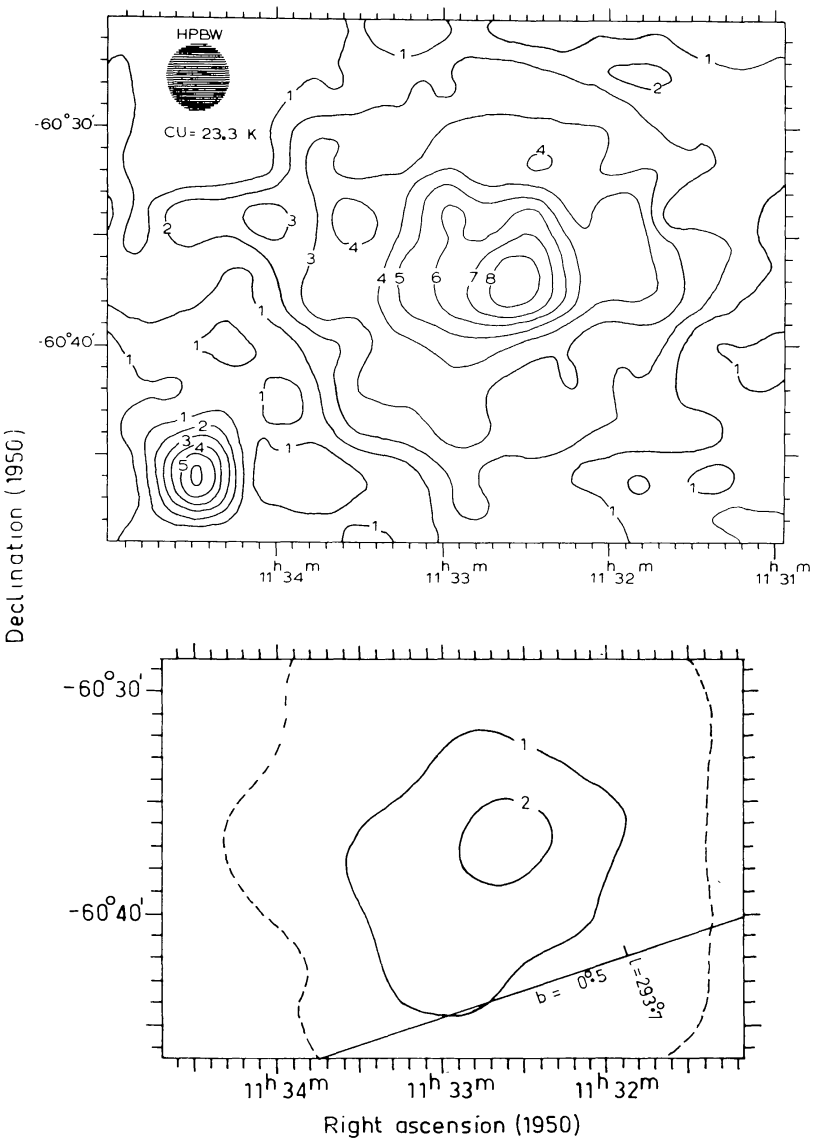

Fig. 1. Contour maps of G293.8+0.6: (*top*) at 408 MHz, (*bottom*) at 5000 MHz (R.A. scans, CU = 0.1 K).

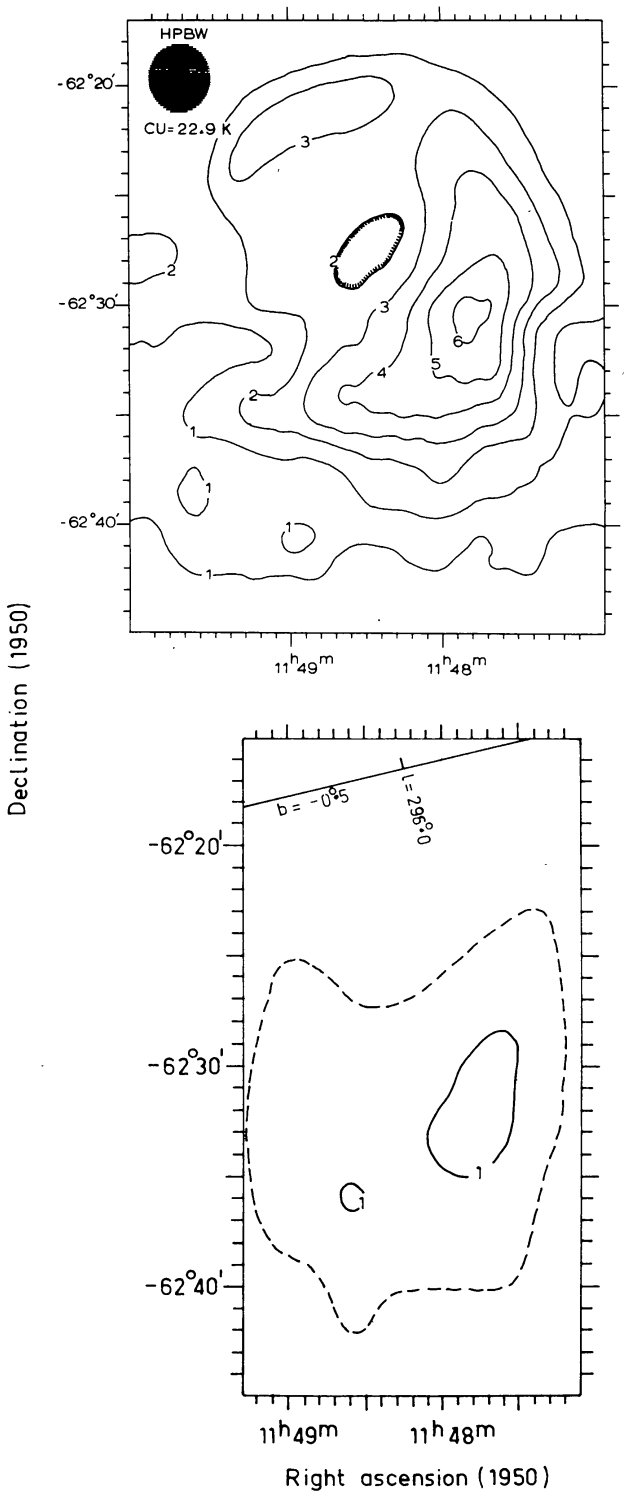

Fig. 2. Contour maps of G296.1–0.7: (*top*) at 408 MHz, (*bottom*) at 5000 MHz (Dec. scans, CU = 0.1 K).

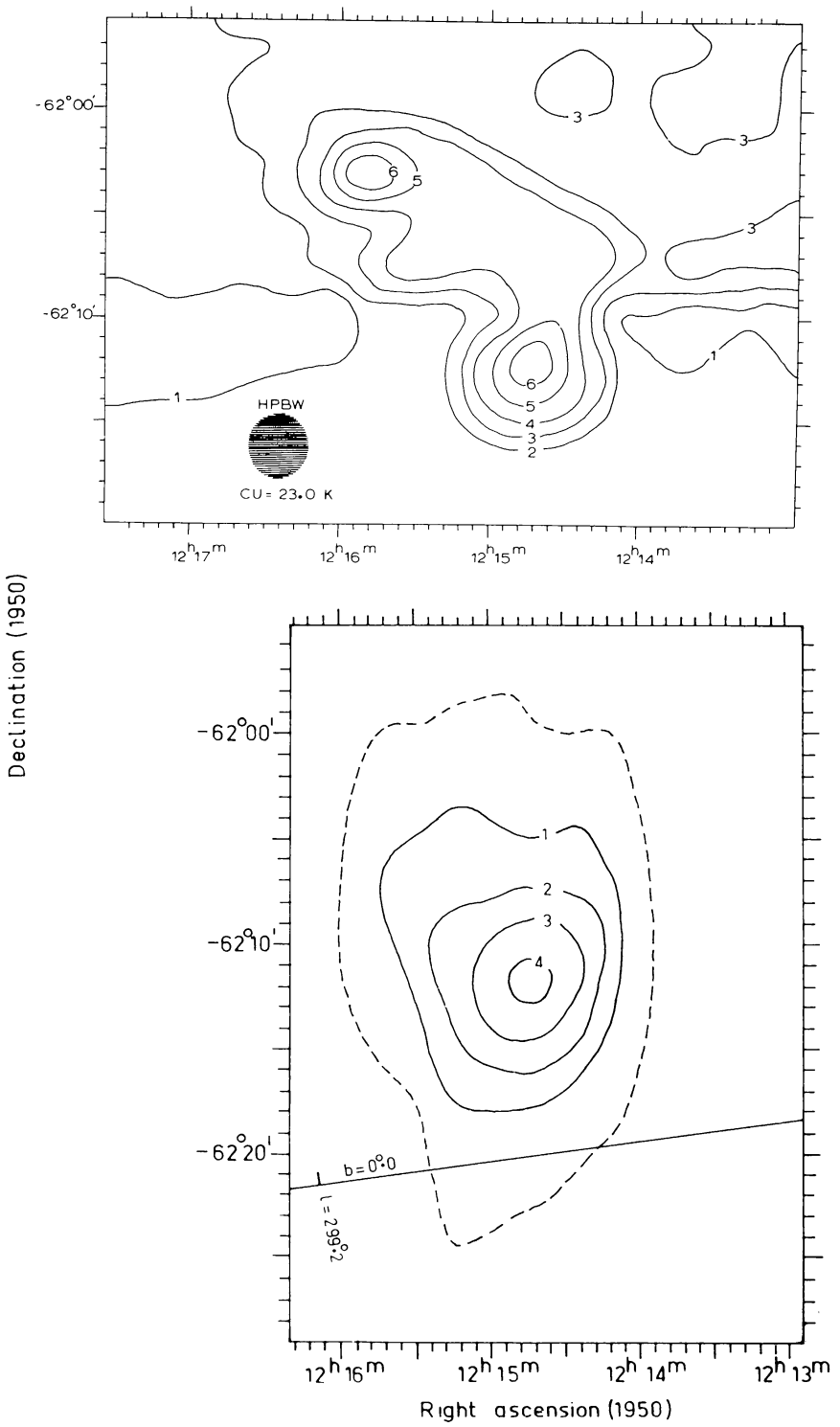

Fig. 3. Contour maps of G299.0+0.2: (*top*) at 408 MHz, (*bottom*) at 5000 MHz (Dec. scans, CU = 0.2 K).

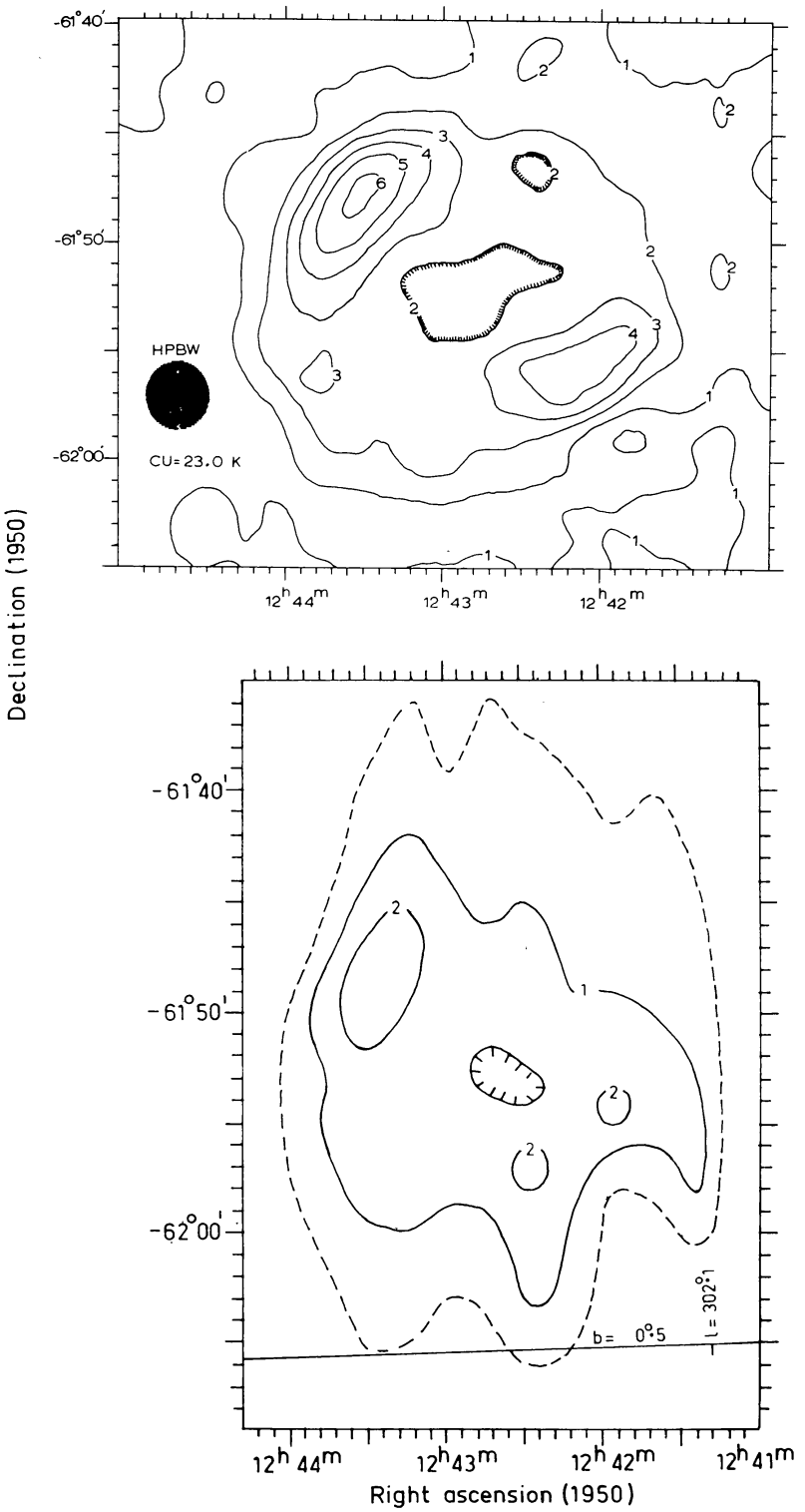

Fig. 4. Contour maps of G302.3+0.7: (*top*) at 408 MHz, (*bottom*) at 5000 MHz (Dec. scans, CU = 0.1 K).

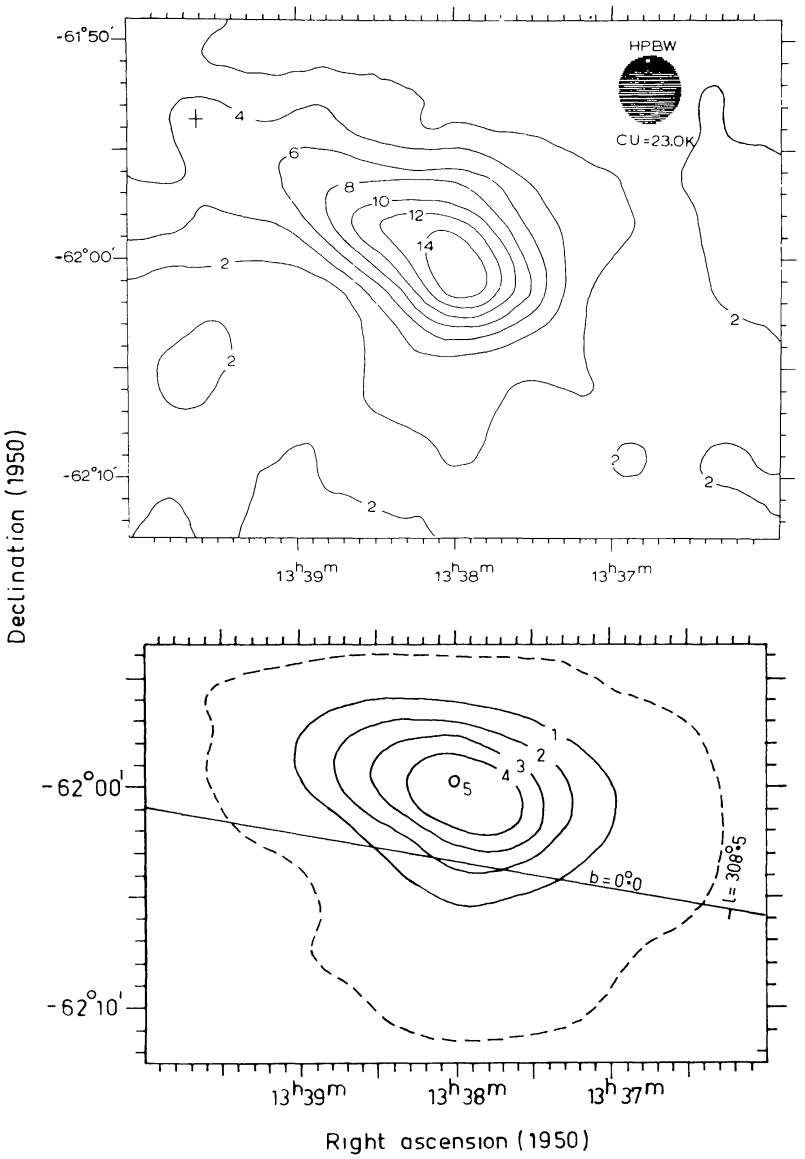

Fig. 5. Contour maps of G308.7+0.0: (*top*) at 408 MHz, (*bottom*) at 5000 MHz (R.A. scans, CU = 0.2 K). On the 408 MHz map, the cross marks the position of the OH emission source OH 308.9+0.1.

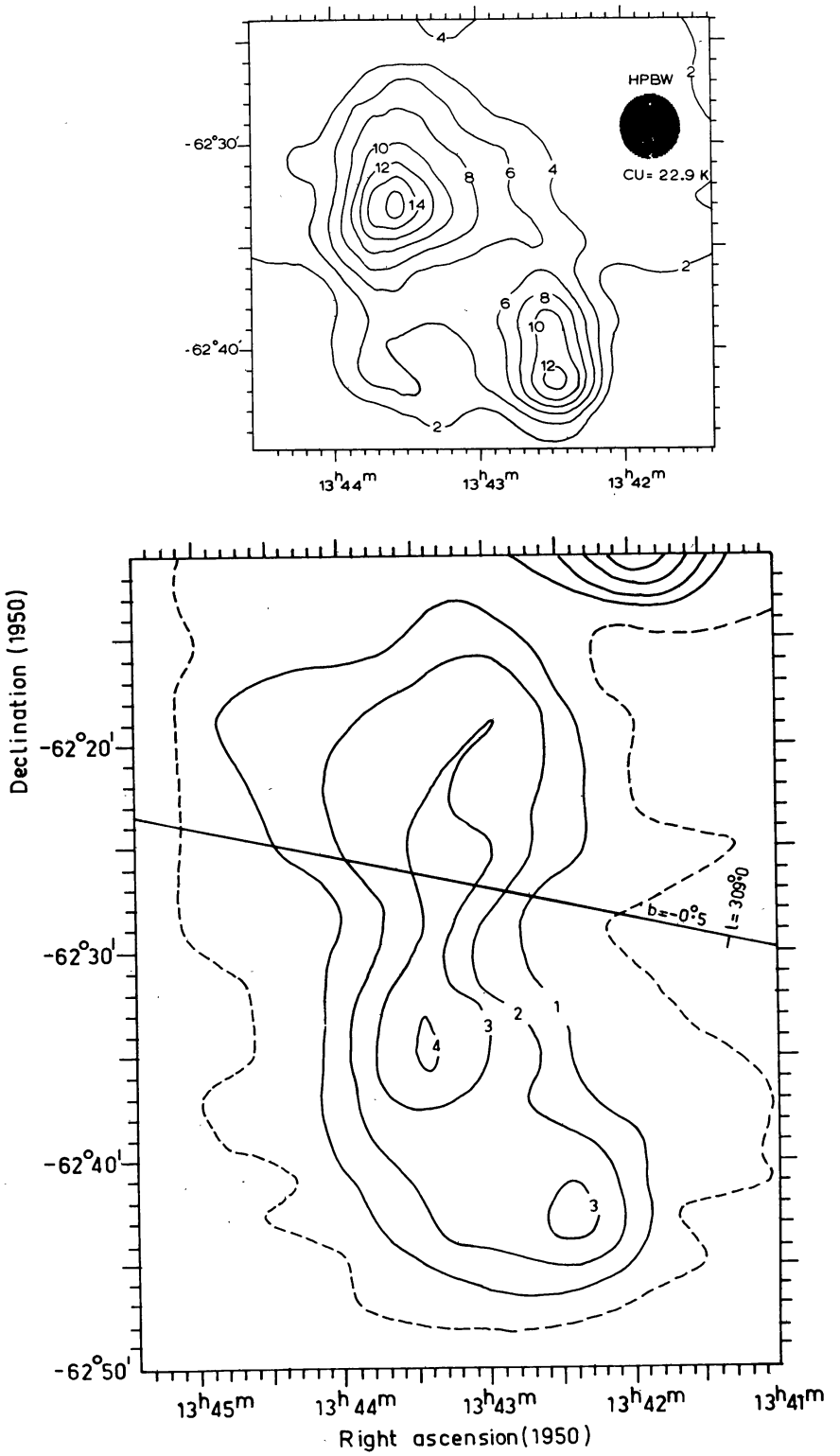

Fig. 6. Contour maps of G309.2–0.6: (*top*) at 408 MHz, (*bottom*) at 5000 MHz (R.A. scans, CU = 0.1 K).

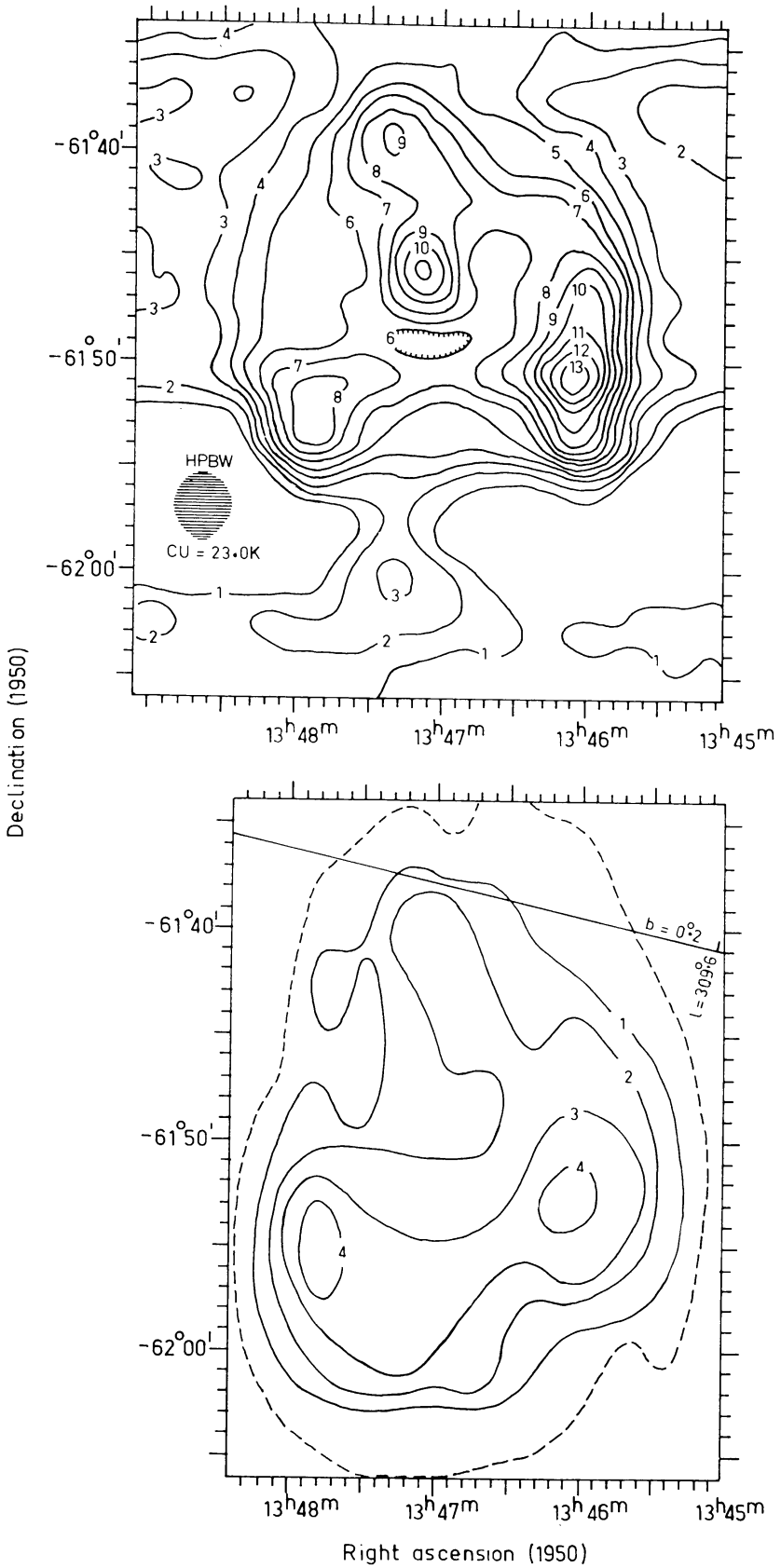

Fig. 7. Contour maps of G309.8+0.0: (*top*) at 408 MHz, (*bottom*) at 5000 MHz (Dec. scans, CU = 0.1 K).

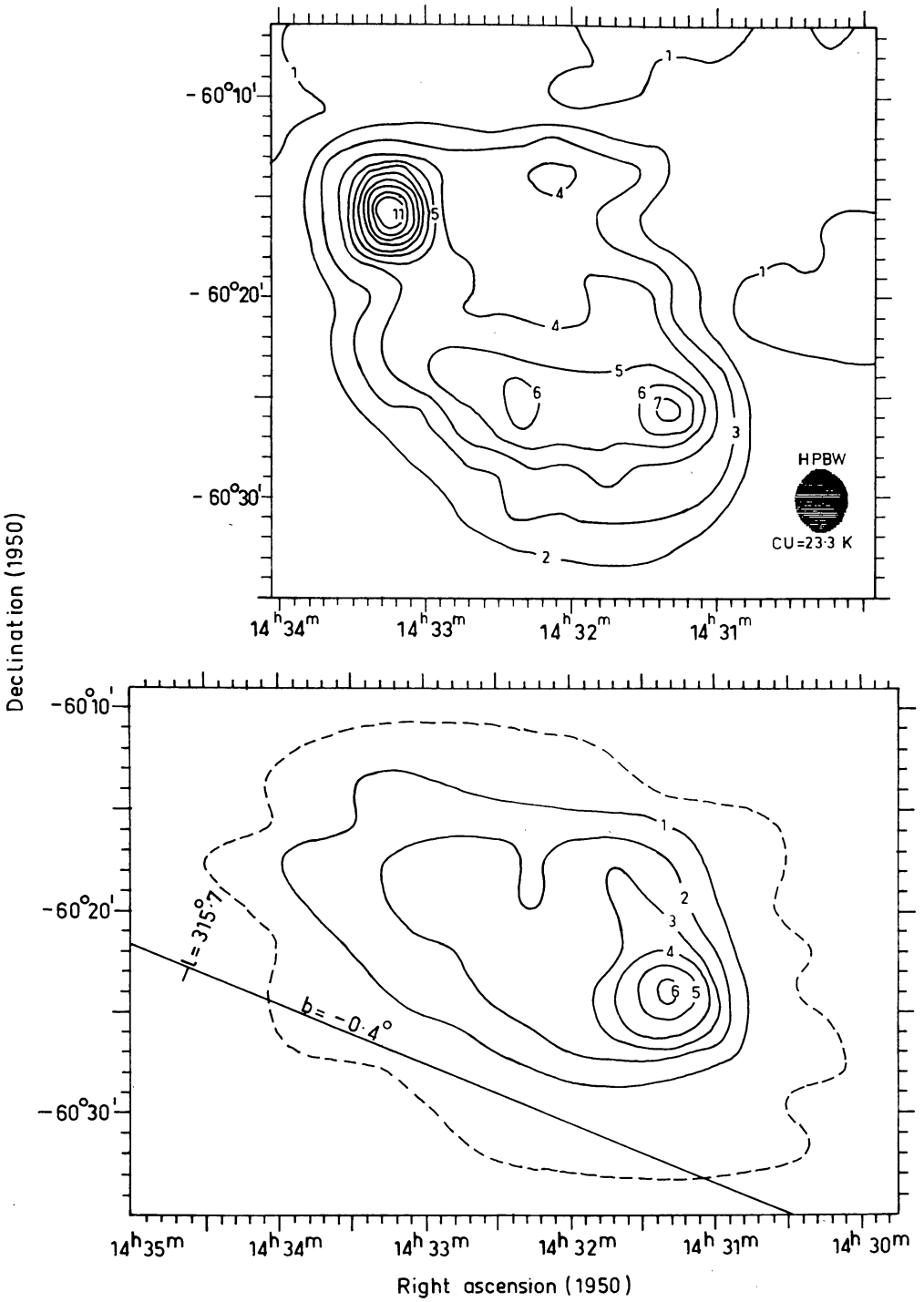

Fig. 8. Contour maps of G315.4–0.3: (*top*) at 408 MHz, (*bottom*) at 5000 MHz (R.A. scans, CU = 0.1 K).

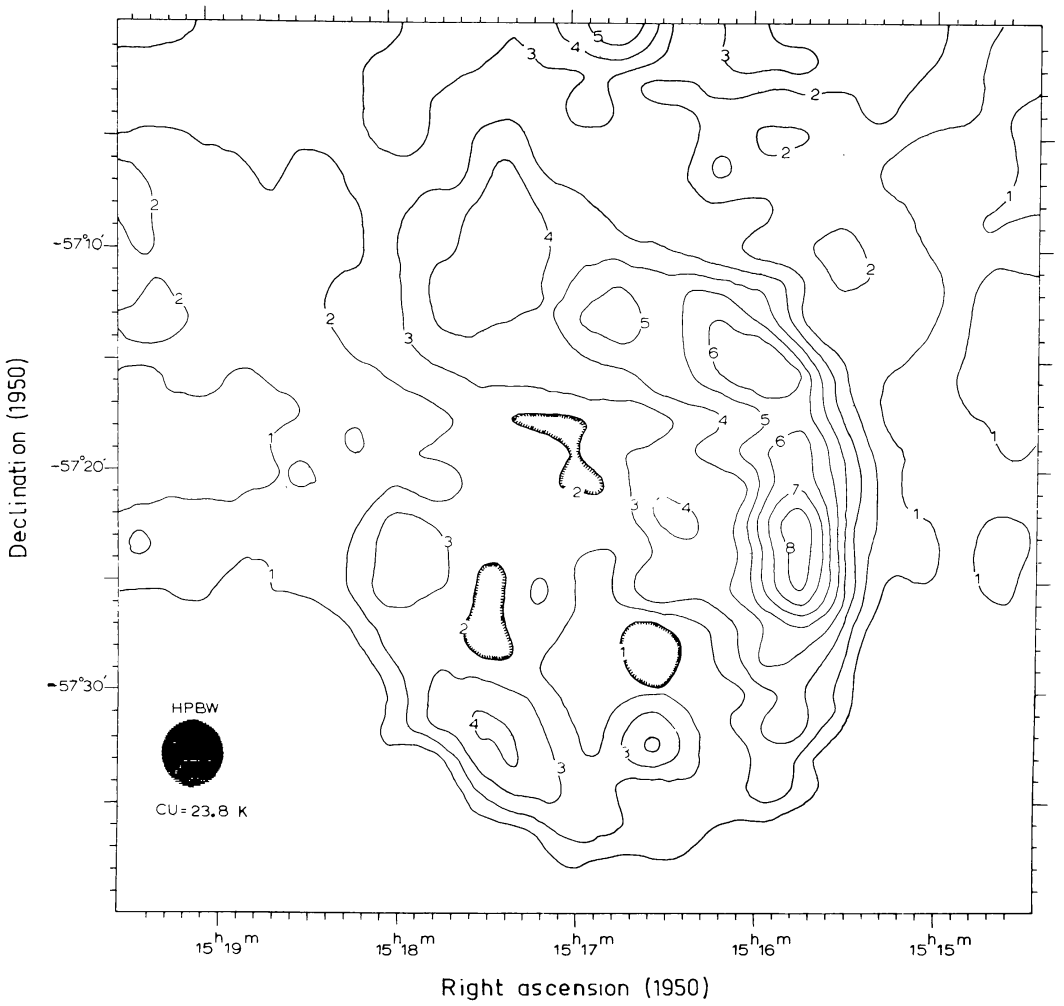

Fig. 9*a*. Contour map of G321.9−0.3 at 408 MHz.

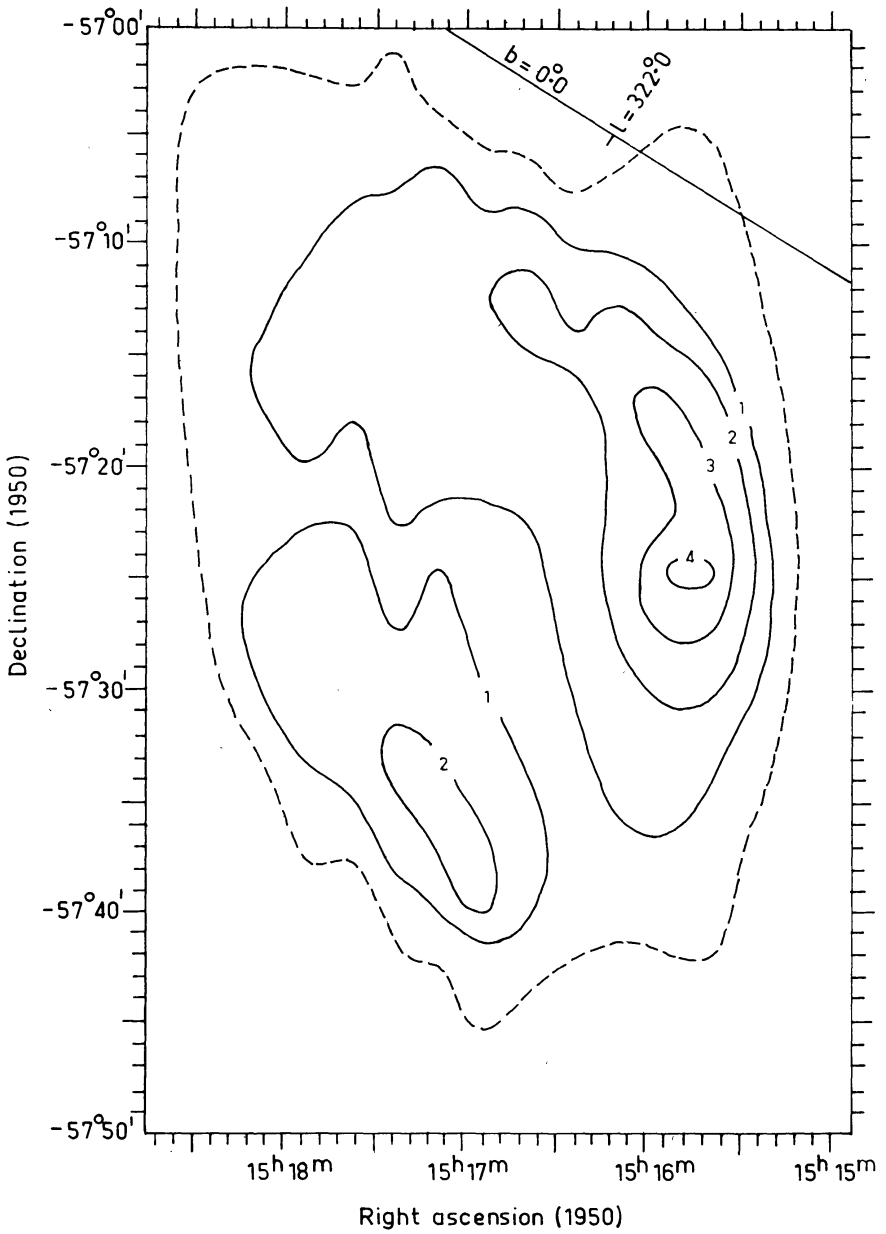

Fig. 9*b*. Contour map of G321.9–0.3 at 5000 MHz (Dec. scans, CU = 0.1 K).

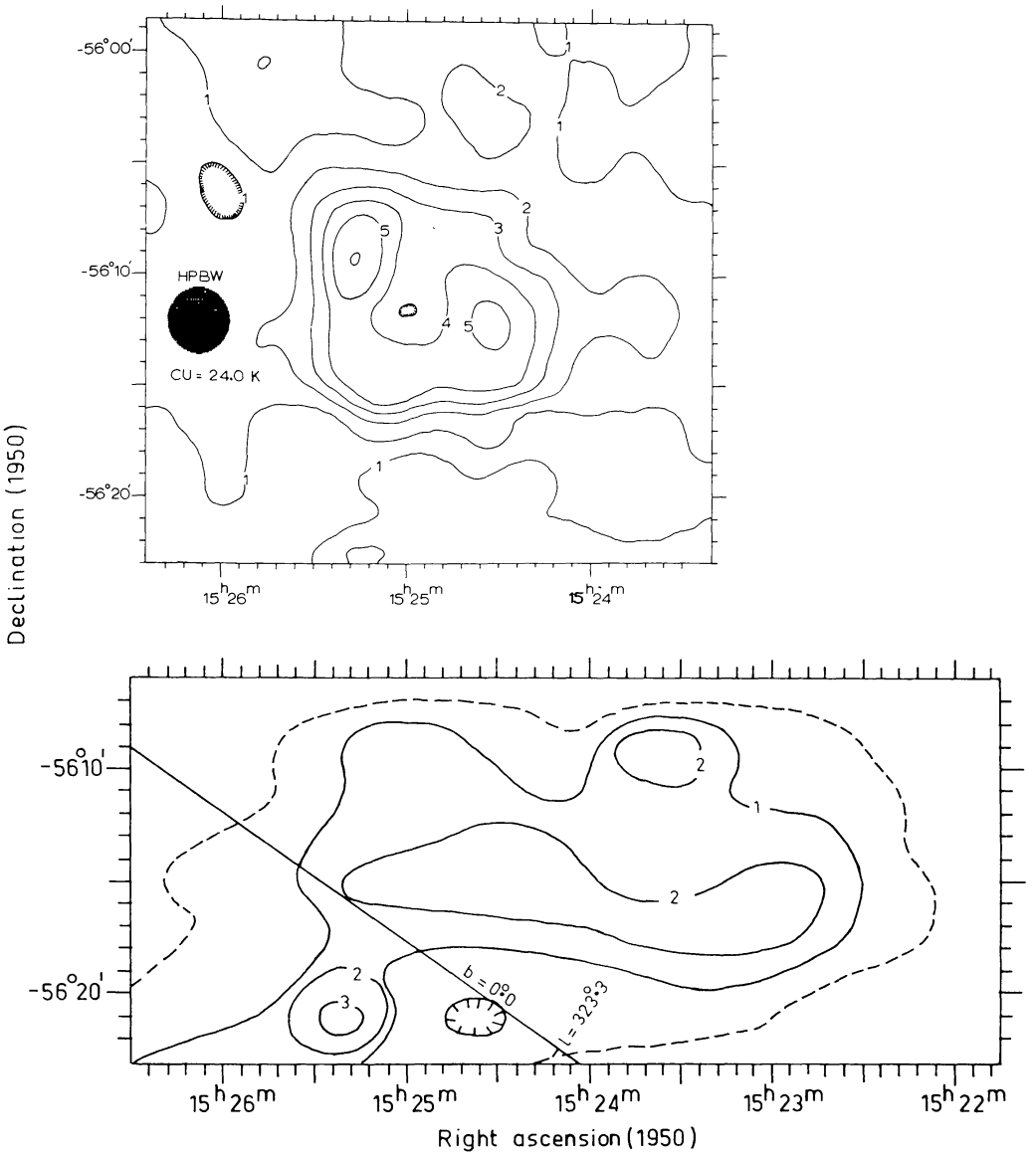

Fig. 10. Contour maps of G323.5+0.1: (*top*) at 408 MHz, (*bottom*) at 5000 MHz (R.A. scans, CU = 0.1 K).

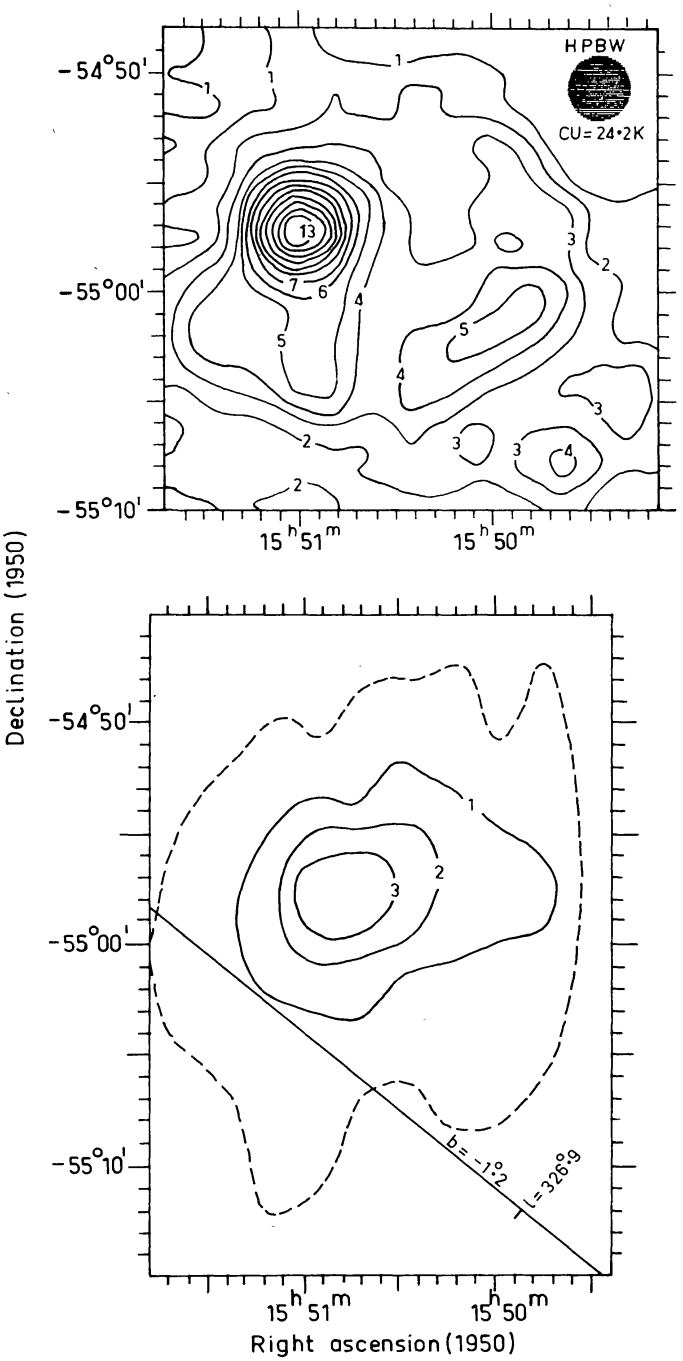

Fig. 11. Contour maps of G327.1−1.1: (*top*) at 408 MHz, (*bottom*) at 5000 MHz (Dec. scans, CU = 0.2 K).

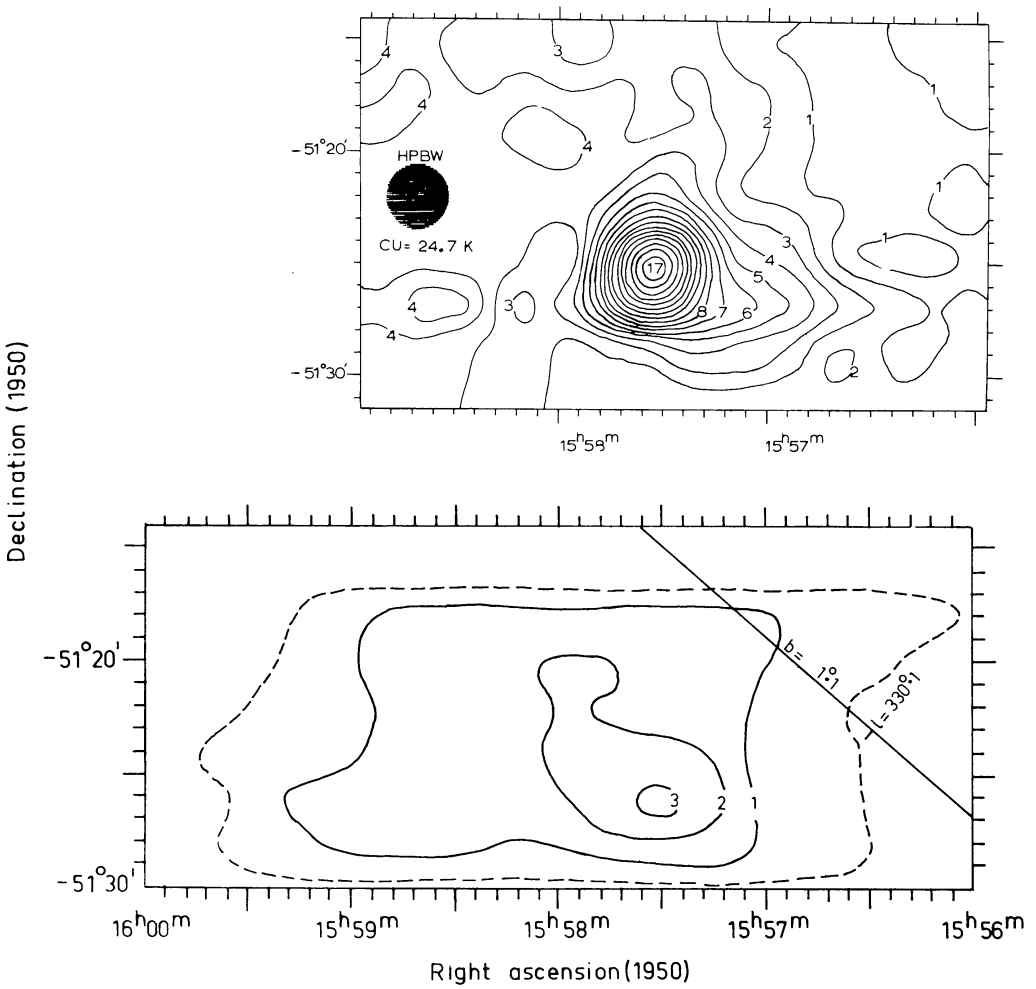

Fig. 12. Contour maps of G330.2+1.0: (*top*) at 408 MHz, (*bottom*) at 5000 MHz (R.A. scans, CU = 0.2 K).

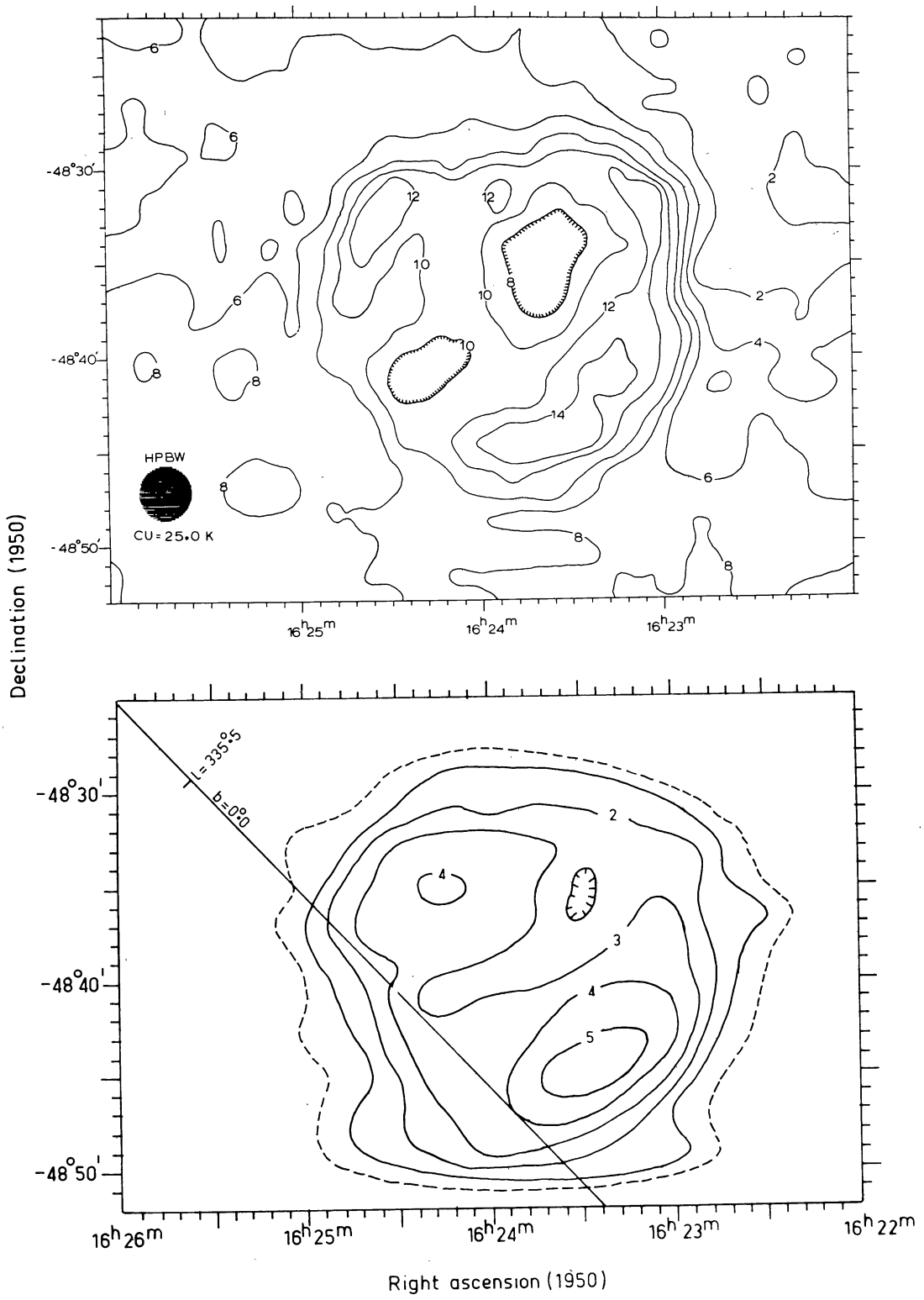

Fig. 13. Contour maps of G335.2+0.1: (*top*) at 408 MHz, (*bottom*) at 5000 MHz (R.A. scans, CU = 0.1 K).

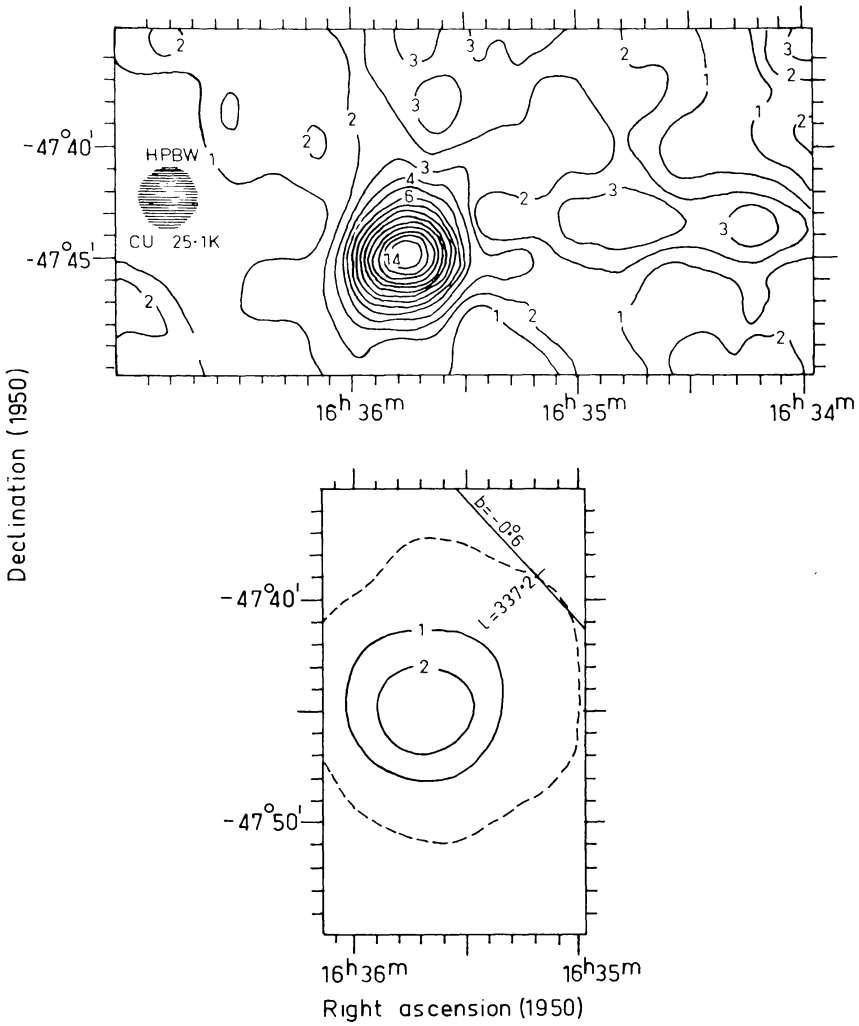

Fig. 14. Contour maps of G337.2–0.7: (*top*) at 408 MHz, (*bottom*) at 5000 MHz (Dec. scans, CU = 0.1 K).

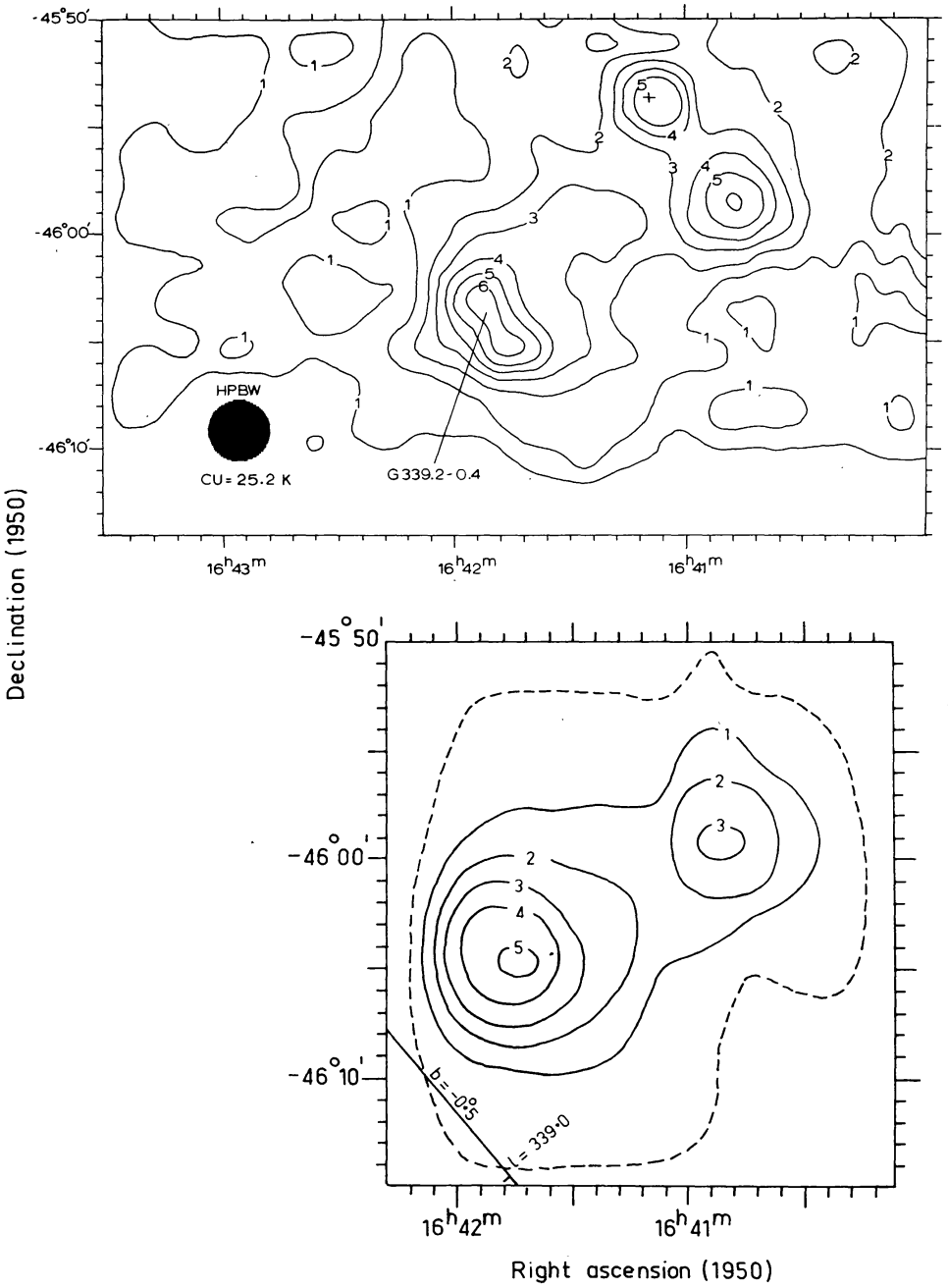

Fig. 15. Contour maps of G339.2–0.4: (*top*) at 408 MHz, (*bottom*) at 5000 MHz (Dec. scans, CU = 0.2 K). The position of the pulsar 1641–45 is marked by a cross on the 408 MHz map.

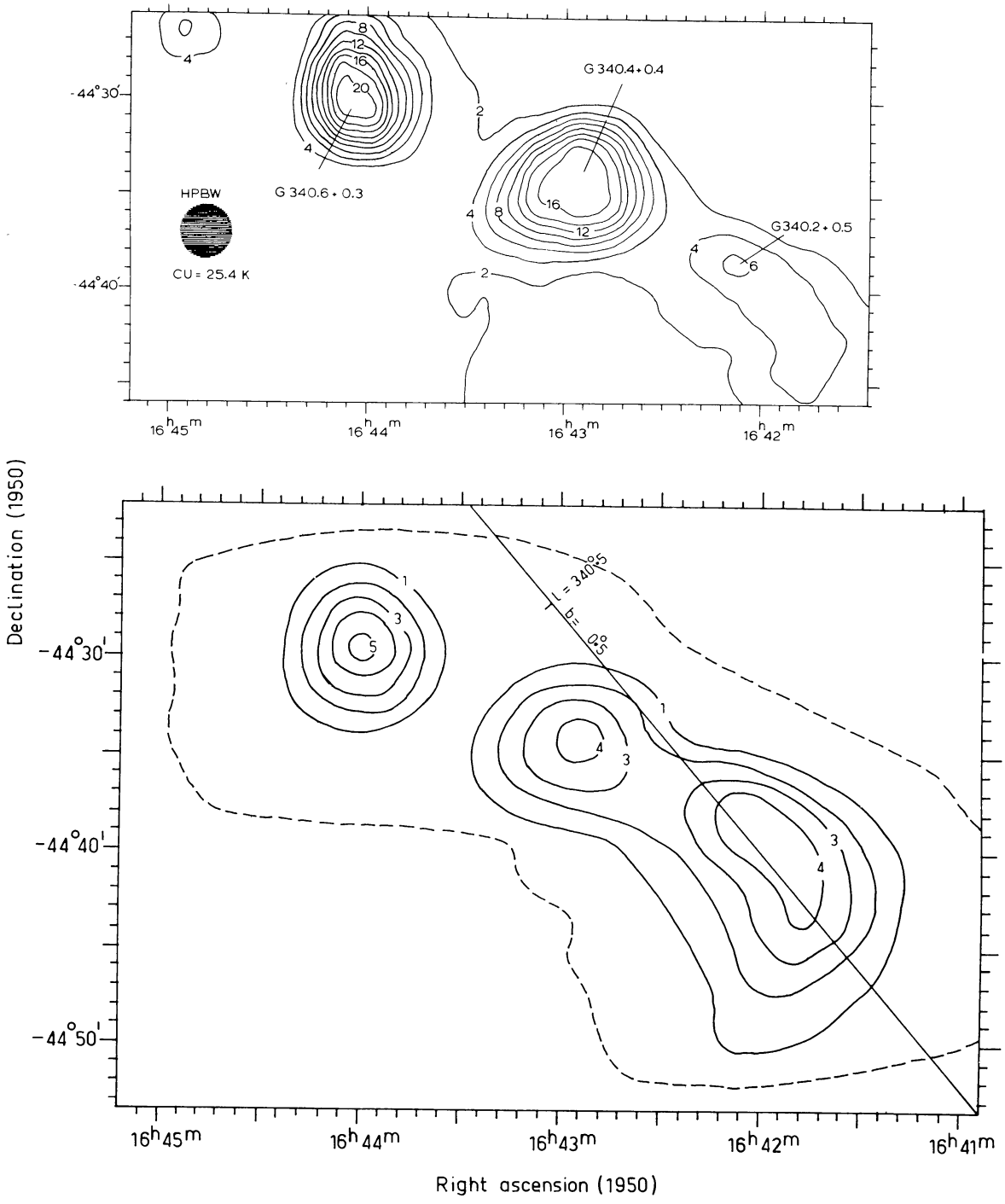

Fig. 16. Contour maps of G340.6+0.3 and G340.4+0.4: (*top*) at 408 MHz, (*bottom*) at 5000 MHz (R.A. scans, CU = 0.2 K).

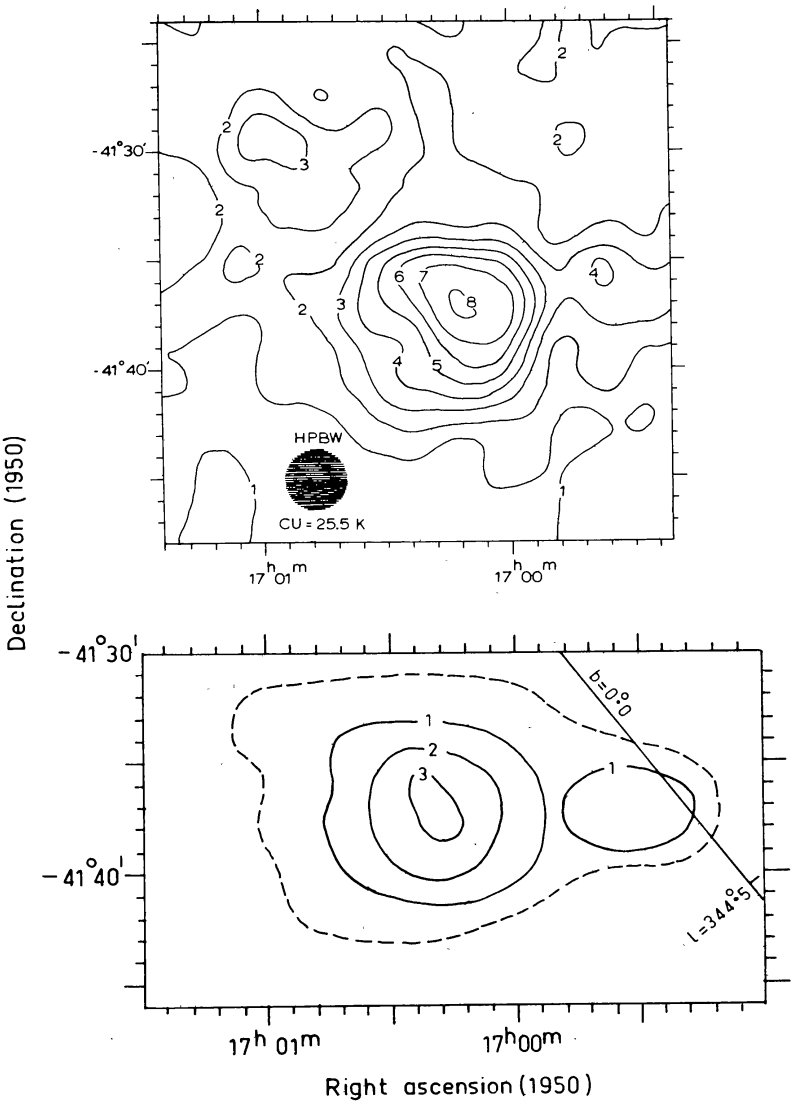

Fig. 17. Contour maps of G344.7–0.1: (*top*) at 408 MHz, (*bottom*) at 5000 MHz (R.A. scans, CU = 0.1 K).

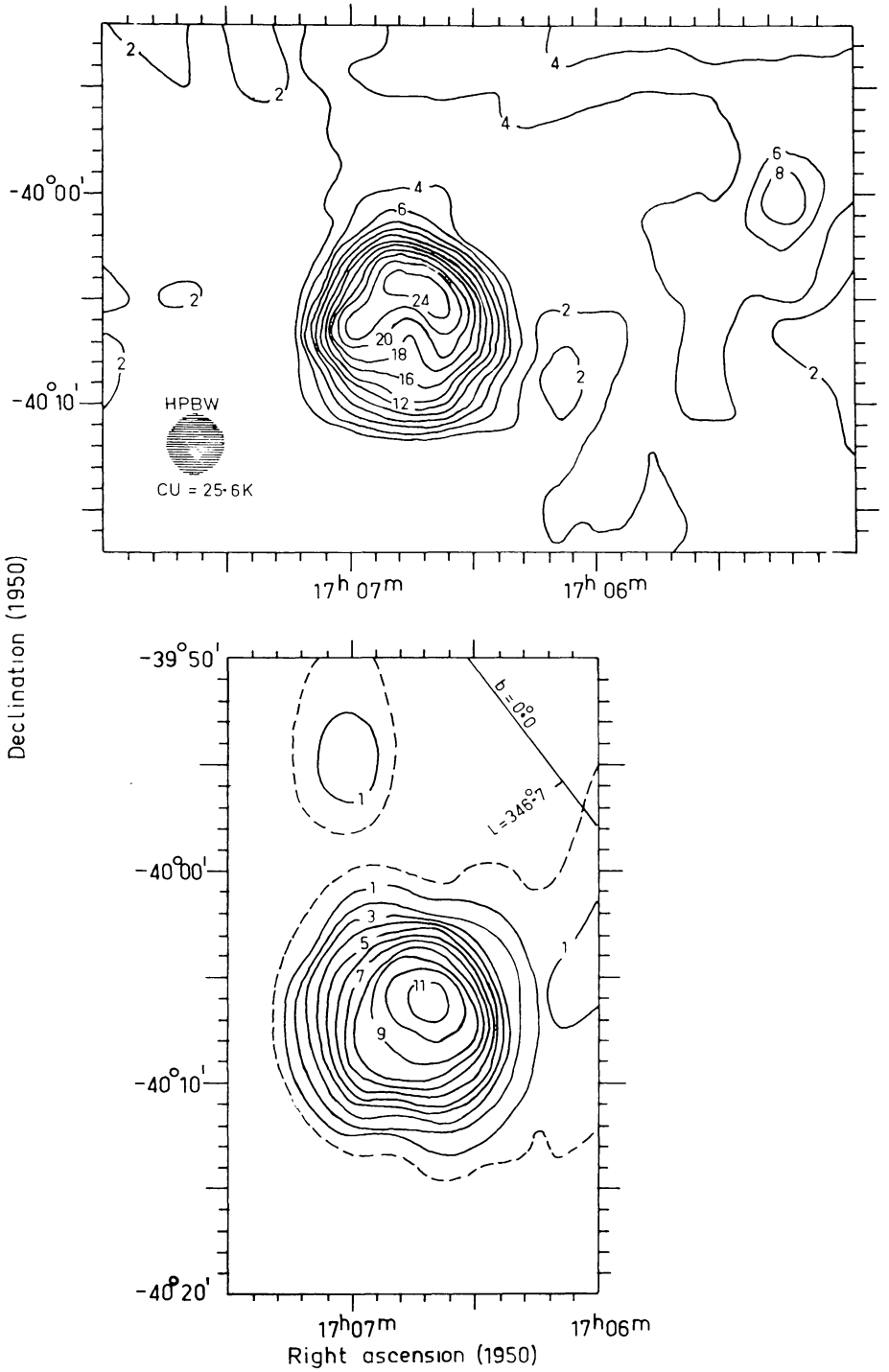

Fig. 18. Contour maps of G346.6–0.2: (*top*) at 408 MHz, (*bottom*) at 5000 MHz (Dec. scans, CU = 0.1 K).

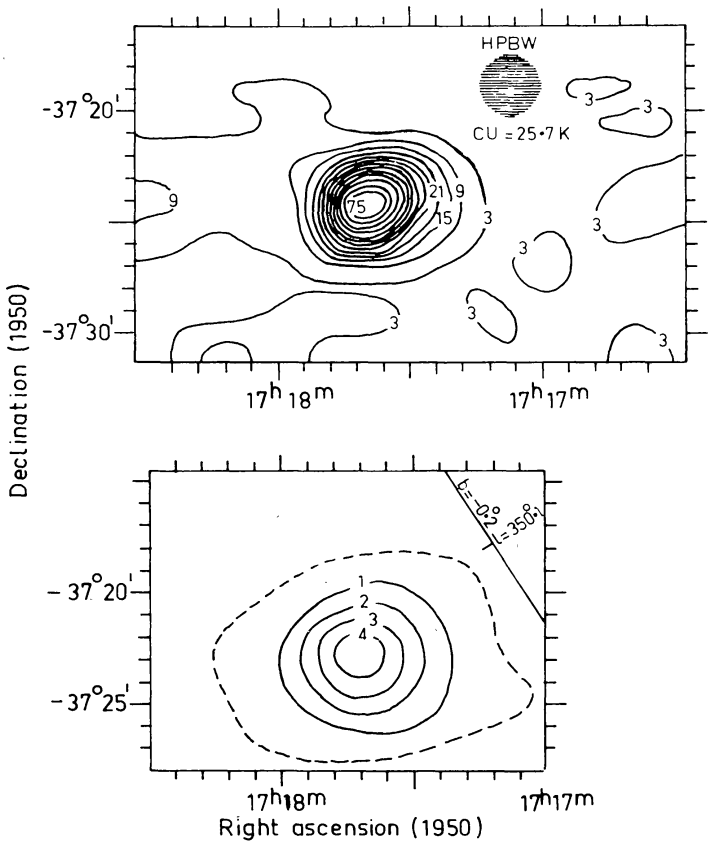

Fig. 19. Contour maps of G350.1–0.3: (*top*) at 408 MHz, (*bottom*) at 5000 MHz (R.A. scans, CU = 0.2 K).

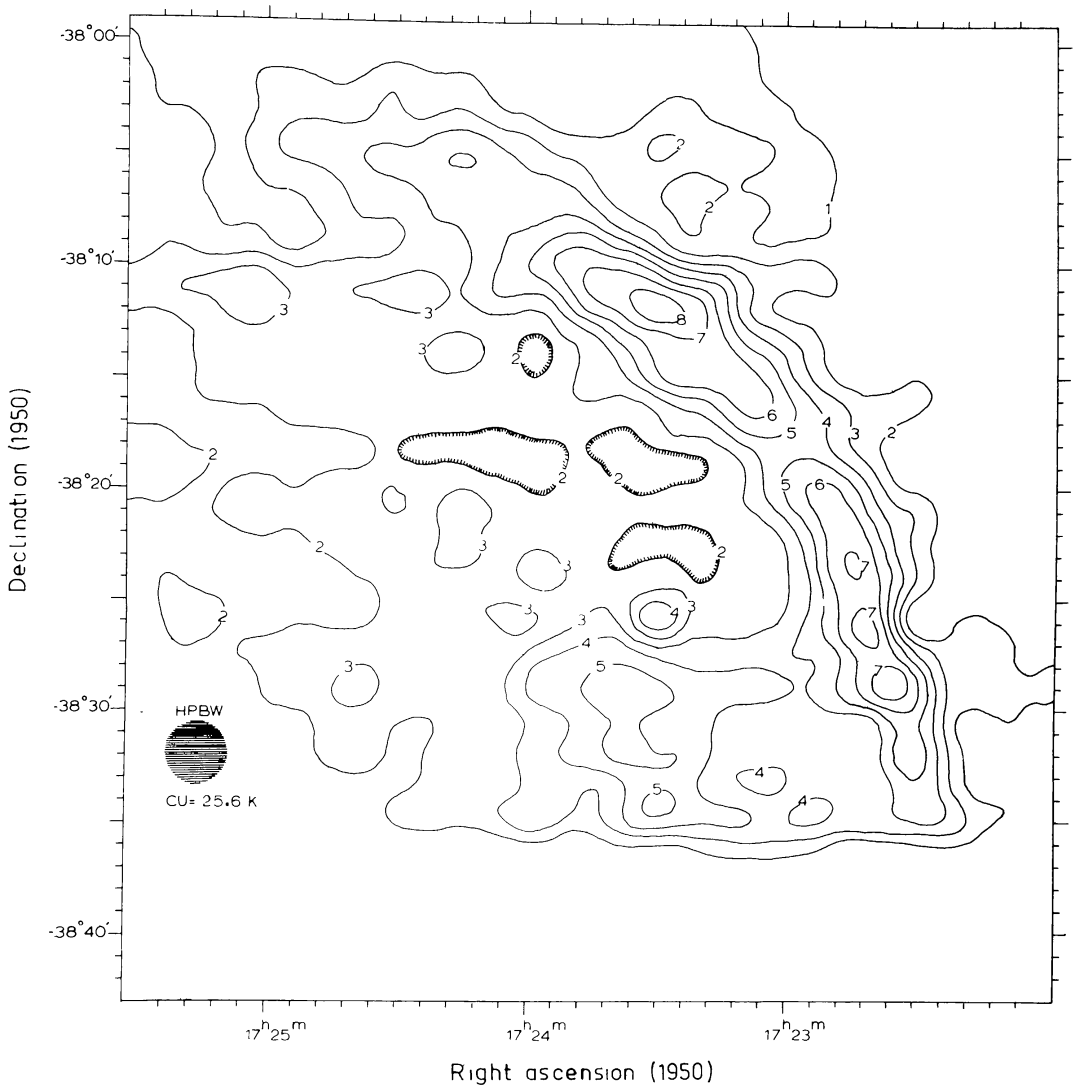

Fig. 20*a*. Contour map of G350.0–1.8 at 408 MHz.

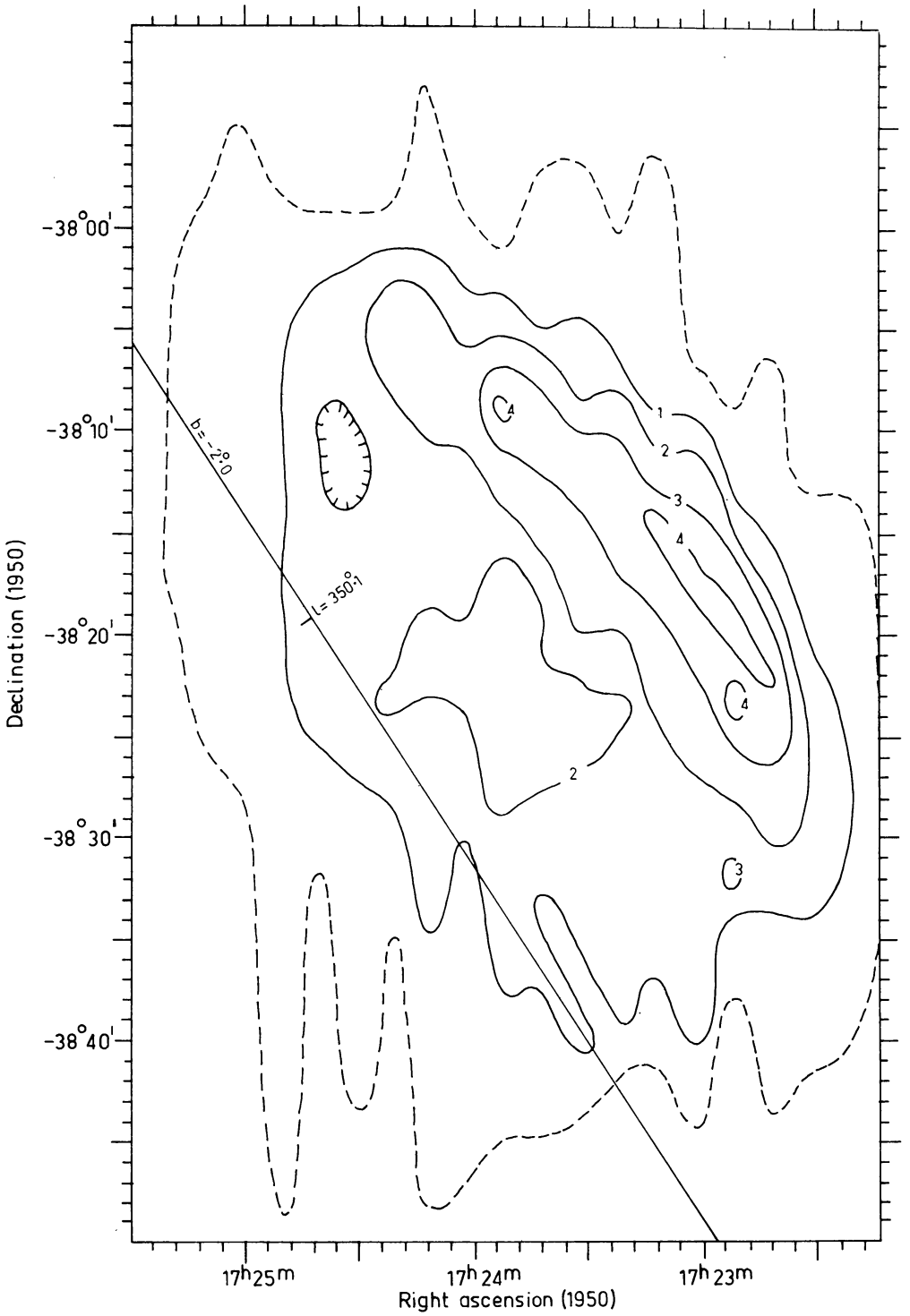

Fig. 20*b*. Contour map of G350.0–1.8 at 5000 MHz (Dec. scans, CU = 0.1 K).

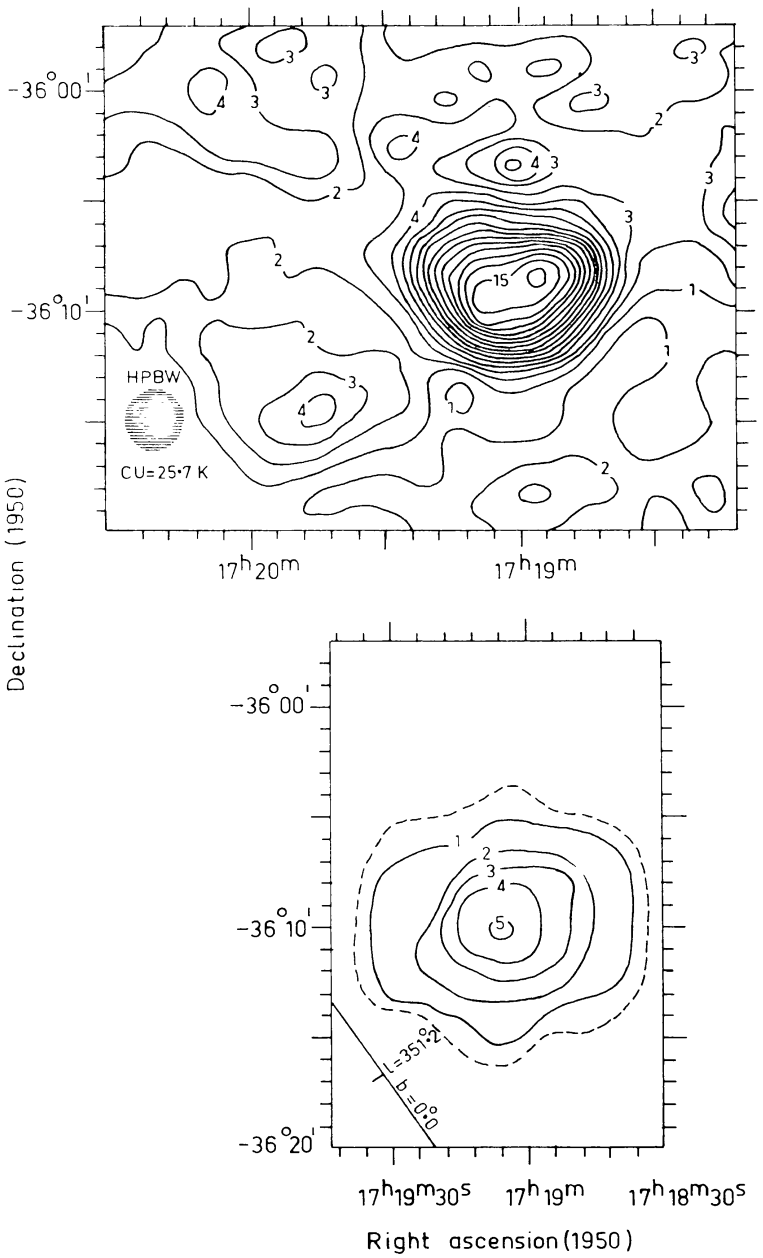

Fig. 21. Contour maps of G351.2+0.1: (*top*) at 408 MHz, (*bottom*) at 5000 MHz (Dec. scans, CU = 0.2 K).

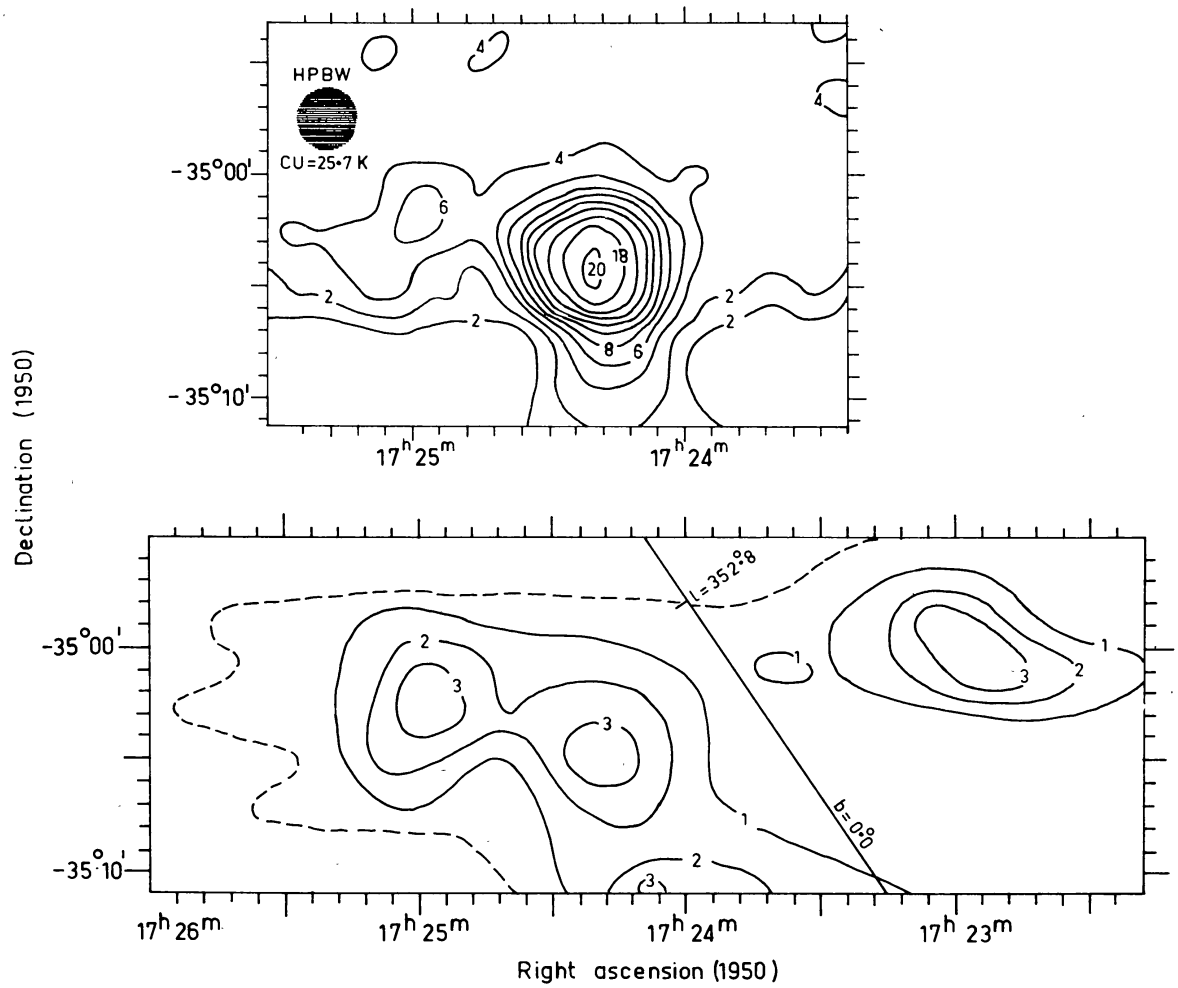

Fig. 22. Contour maps of G352.7−0.1: (*top*) at 408 MHz, (*bottom*) at 5000 MHz (R.A. scans, CU = 0.2 K).

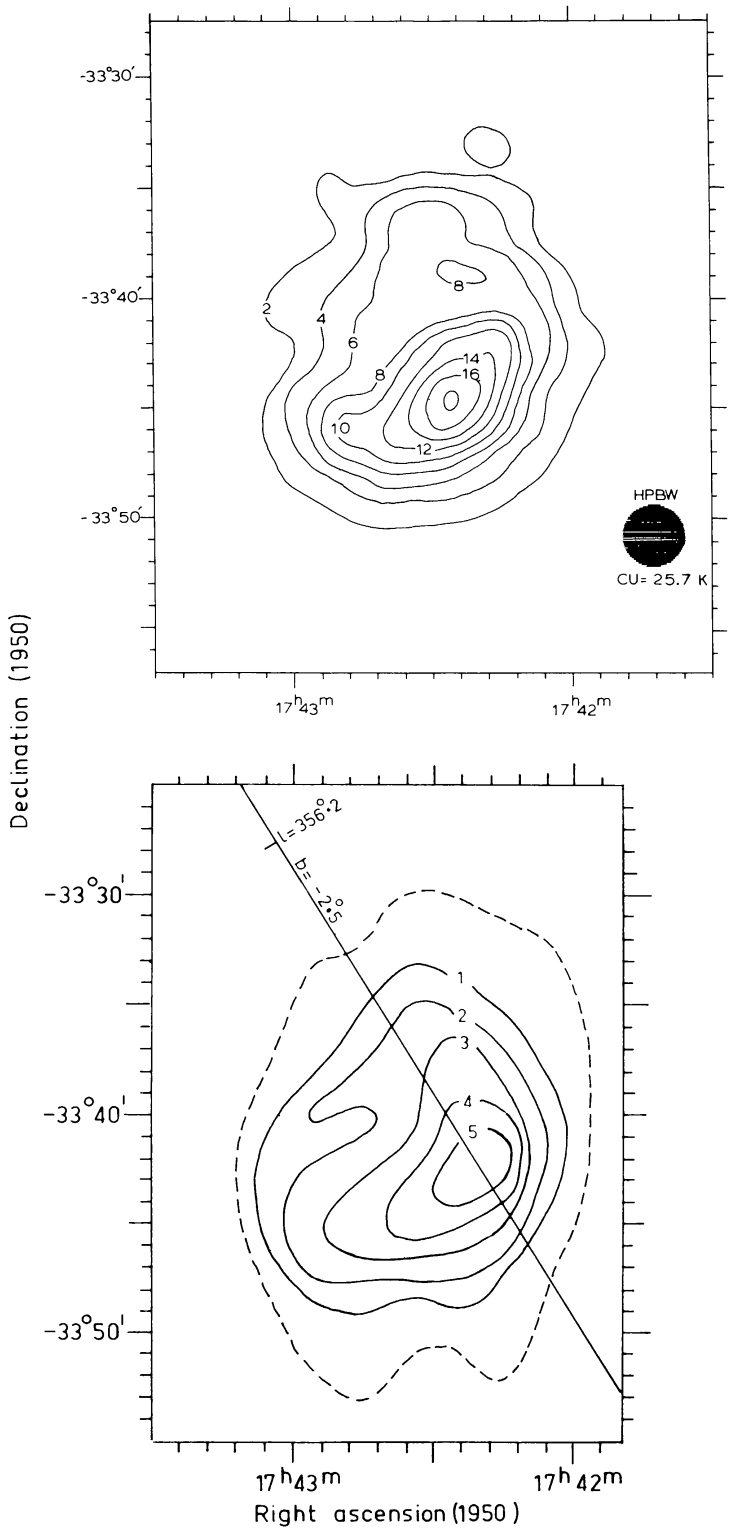

Fig. 23. Contour maps of G355.9–2.5: (*top*) at 408 MHz, (*bottom*) at 5000 MHz (Dec. scans, CU = 0.1 K).

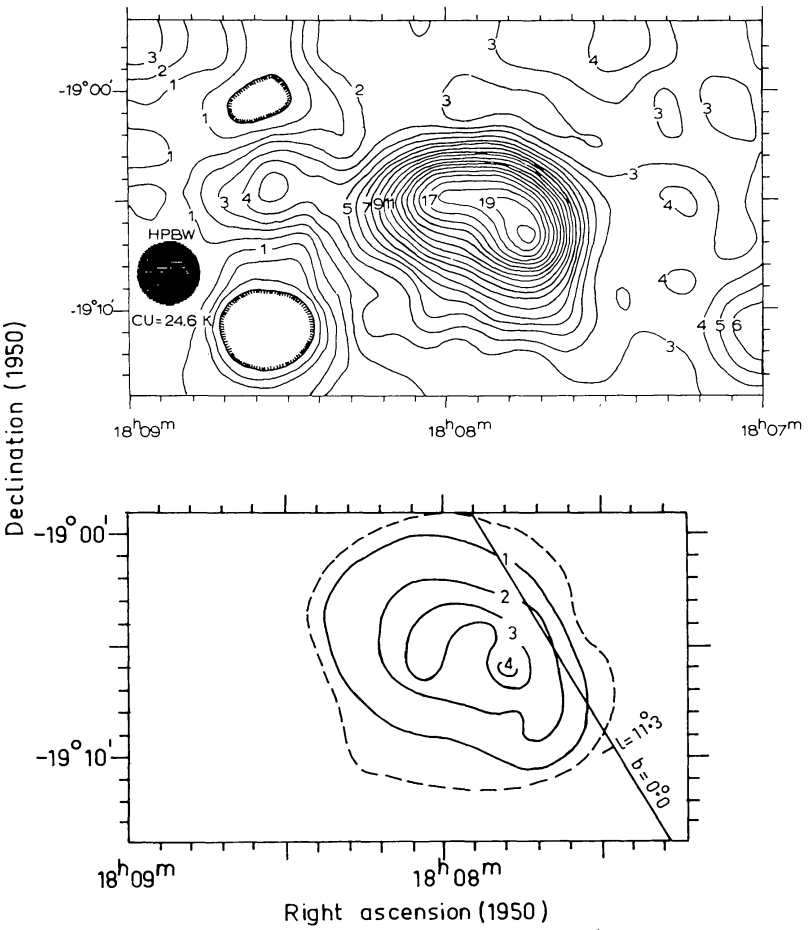

Fig. 24. Contour maps of G11.4–0.1: (*top*) at 408 MHz, (*bottom*) at 5000 MHz (R.A. scans, CU = 0.2 K).

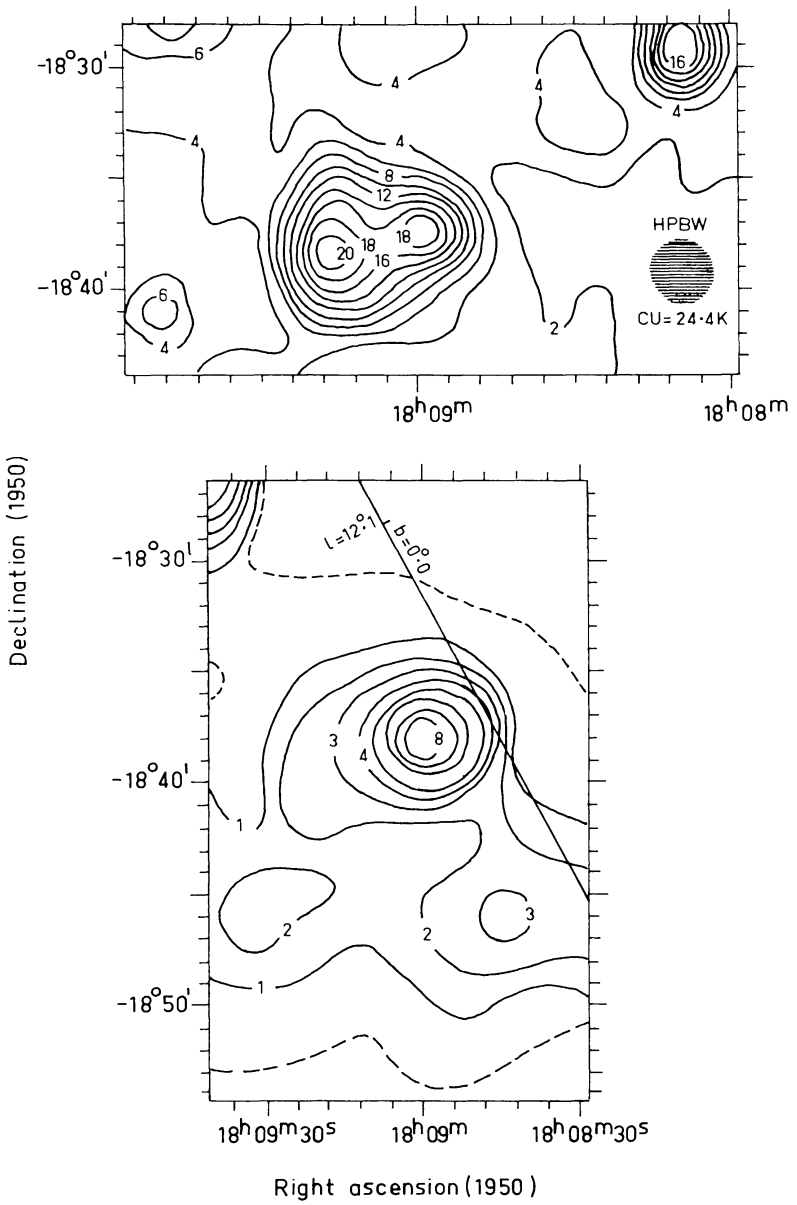

Fig. 25. Contour maps of G12.0–0.1: (*top*) at 408 MHz, (*bottom*) at 5000 MHz (Dec. scans, CU = 0.2 K).

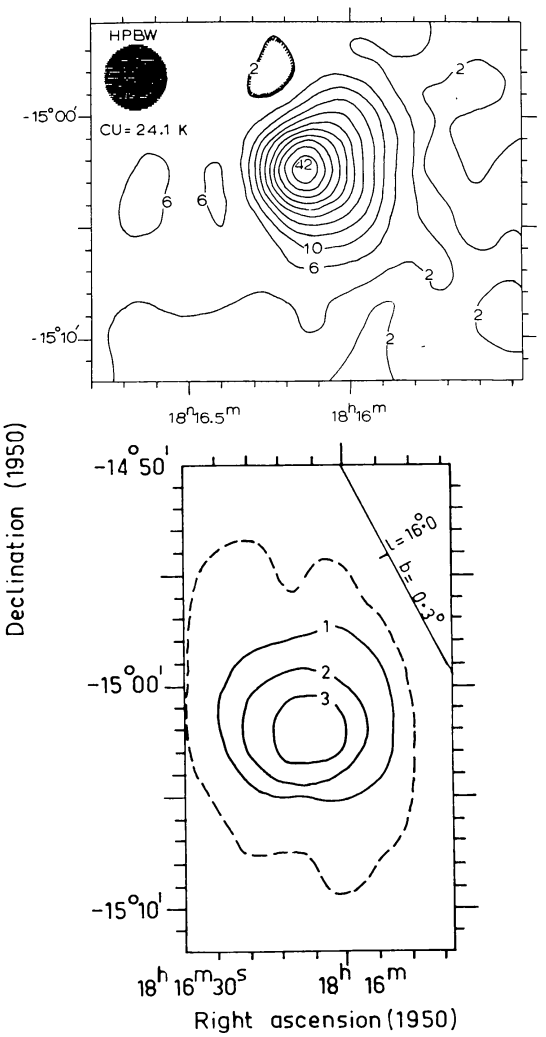

Fig. 26. Contour maps of G15.9+0.2: (*top*) at 408 MHz, (*bottom*) at 5000 MHz (Dec. scans, CU = 0.2 K).

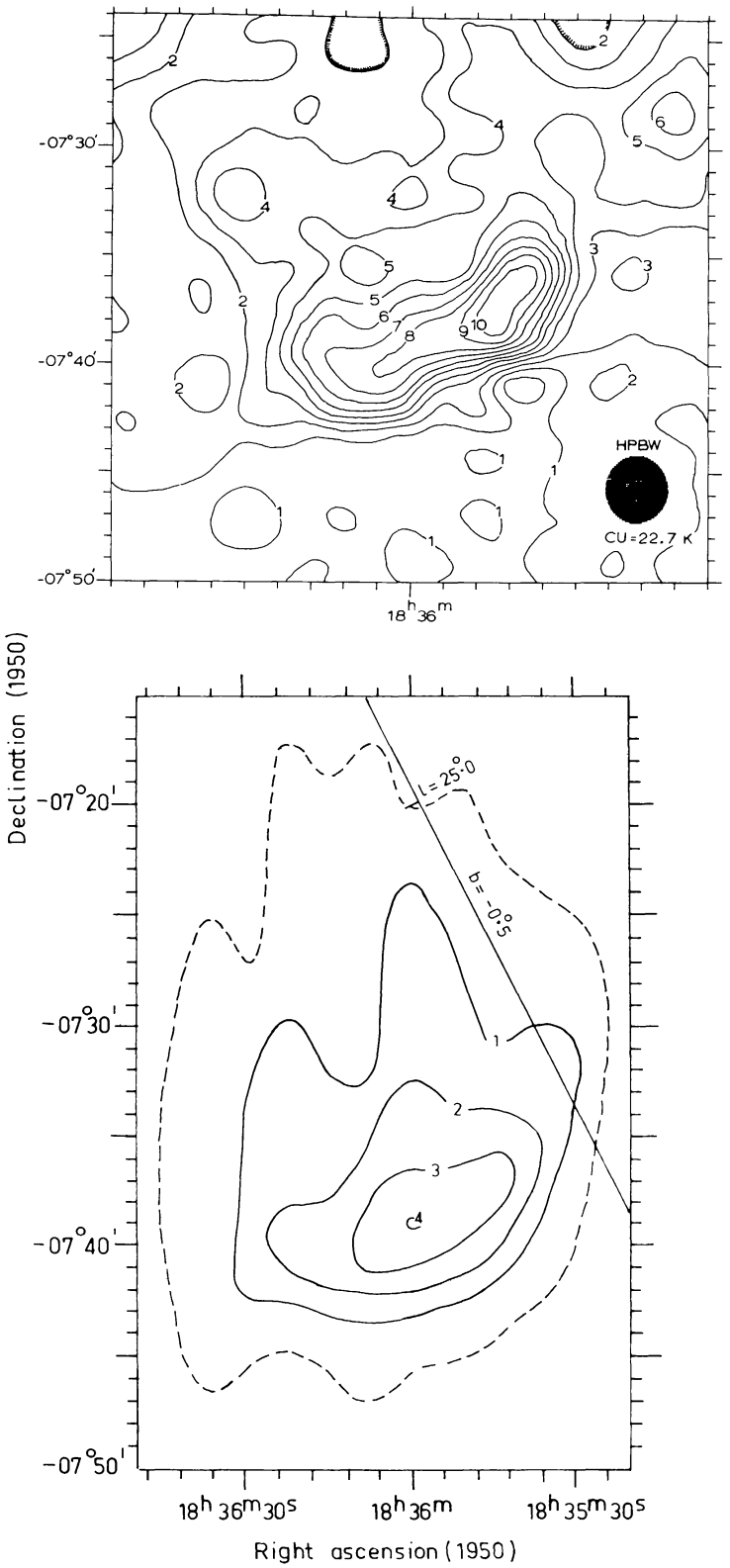

Fig. 27. Contour maps of G24.7–0.6: (*top*) at 408 MHz, (*bottom*) at 5000 MHz (Dec. scans, CU = 0.1 K).